NEUTRONICS ANALYSES OF DISPERSION FUELS FOR CORE CONVERSION OF NIRR-1

A PHD FINAL REPORT SUBMITTED TO THE DEPARTMENT OF PHYSICS, AHMADU BELLO UNIVERSITY, ZARIA

BY

ISAAC KOLAWOLE IBIKUNLE

DEPARTMENT OF PHYSICS

FACULTY OF PHSYICAL SCIENCES

AHMADU BELLO UNIVERSITY

ZARIA, NIGERIA

JULY 2018

Title Page

NEUTRONICS ANALYSES OF DISPERSION FUELS FOR CORE CONVERSION OF NIRR-1

BY

ISAAC KOLAWOLE IBIKUNLE (B.Sc., M.Sc., MBA)

PHD/SCI/41313/2012-2013

A PROJECT THESIS SUBMITTED TO THE SCHOOL OF POSTGRADUATE STUDIES, AHMADU BELLO UNIVERSITY IN PARTIAL FULFILMENT FOR THE AWARD OF DOCTOR OF PHILOSOPHY IN PHYSICS

DEPARTMENT OF PHYSICS

AHMADU BELLO UNIVERSITY

ZARIA, NIGERIA

JULY 2018

Declaration Page

I declare that the work in this Project Thesis titled “Neutronics Analyses of Dispersion Fuels for Core Conversion of NIRR-1” has been performed out by me in the Department of Physics. The information derived from literature has been duly acknowledged in the text and a list of references provided. No part of this project thesis was previously presented for another degree or diploma at this or any other Institution.

Isaac Kolawole IBIKUNLE

_____ _____ _____

Certification Page

This project thesis entitled "NEUTRONICS ANALYSES OF DISPERSION FUELS FOR CORE CONVERSION OF NIRR-1" by Isaac Kolawole IBIKUNLE meets the regulations governing the award of the degree of Doctor Philosophy in Physics of Ahmadu Bello University, and is approved for its contribution to knowledge and literary presentation.

Prof. S. A. Jonah
Chairman, Supervisory Committee _____ _____

Prof. G. B. Balogun
Member, Supervisory Committee _____ _____

Dr. U. Sadiq
Member, Supervisory Committee _____ _____

Prof. N. Rabiu
Head of Department _____ _____

Prof. S. Z. Abubakar
Dean, School of Postgraduate Studies _____ _____

Acknowledgement Page

My sincere gratitude to my major supervisor Prof. S.A. Jonah for his guidance and leadership, and to the members of my supervisory committee, Prof G.I. Balogun and Dr. U. Sadiq for their support in overcoming the challenges faced during this research.

My appreciation also goes to my friends and colleagues in the Department of Physics and Center for Energy Research and Training for their valuable feedback, logistical contributions, and encouragement. Special mention to Dr. Y.V. Ibrahim, Prof. CK. Daudu, Prof. K.M. Lawal, Dr. T. Olugbemi and Mr. B. Nwosu for their friendship and encouragement which has made this journey somewhat less arduous.

Finally, I would like to thank God Almighty for the granting me the strength to preserve and complete this research. Heartfelt gratitude to my family - Royel, Oluwatomisin and Daniel, my mother and my siblings for their cooperation, support and prayers throughout the thesis writing stage.

Abstract

The modification of Miniature Neutron Source Reactor (MNSR) facilities from 90% HEU cores to below 20% LEU systems as part of the on-going worldwide effort of converting Research Reactors from highly enriched uranium (HEU) cores to low enriched uranium (LEU) cores under the auspices of Reduced Enrichment for Research and Test Reactors (RERTR) program. In this work, neutronics feasibility studies of three dispersion fuels have been performed using the Monte Carlo N-Particle Transport (MCNP) code to determine their suitability for the conversion of Nigeria Research Reactor-1 (NIRR-1) from HEU (>90%) to LEU (<20%) fuel. The potential LEU dispersion fuels investigated in this work include U_3Si, U_3Si_2, and U_9Mo, each enriched to 19.75%. The following reactor core physics parameters were computed for the LEU fuel options; clean cold core excess reactivity (ρ_{ex}), control rod (CR) worth, shut down margin (SDM), neutron flux distributions in the irradiation channels and kinetics data (i.e. effective delayed neutron fraction, β_{eff} and prompt neutron lifetime, l_f). Results are compared with experimental and calculated data of the current HEU core and indicate that it would be feasible to use any of the LEU fuel options for the conversion of commercial MNSR in general and NIRR-1 in particular from HEU to LEU.

Title Page ii

Declaration Page iii

Certification Page iv

Acknowledgement Page v

Abstract vi

LIST OF TABLES xi

LIST OF FIGURES xii

1 INTRODUCTION 1

1.1 General Introduction 1

1.2 Statement of the Problem: HEU, LEU, and Proliferation 4

1.3 Purpose of this Study 5

1.4 Significance of the Study 6

1.5 Research Aims and Objectives 6

2 LITERATURE REVIEW/THEORETICAL FRAMEWORK 7

2.1 Interactions of Neutron with Matter 7

2.1.1 Compound Nucleus Formation 7

2.1.2 Potential scattering 9

2.1.3 Direct interaction 9

2.2 Fission neutrons 9

2.3 The Multiplication Factor 10

2.3.1 The four-factor formula 11

2.3.2 The six-factor formula 12

2.4 Reactivity 13

2.4.1 Control of reactivity 13

2.4.2 Coefficients of reactivity 14

2.5 Boltzmann Equation 14

2.5.1 Integral form of the Boltzmann equation 18

2.6 Neutron Cross Section Data Libraries 18

2.6.1 Thermal neutron scattering 20

2.7 The History of the Monte Carlo Method 22

2.8 Monte Carlo and Criticality Calculations 23

2.9 Mathematical Basis for Monte Carlo Simulation 25

2.9.1 Generation of random numbers 25

2.9.2 Probability density function 27

2.9.3 Cumulative distribution function 28

2.10 Sampling Methods 28

2.10.1 Inverse CDF method – continuous distribution 28

2.10.2 Inverse CDF method – discrete distribution 28

2.10.3 Acceptance-rejection method 29

2.10.4 Sampling from the exponential distribution using the inverse CDF method 30

2.11 Law of Large Numbers and Central Limit Theorem 30

2.12 MCNP Statistics 32

2.12.1 Relative error 32

2.12.2 Figure of merit (FOM) 33

2.12.3 Variance of variance (VOV) 33

2.13 Variance Reduction 34

2.13.1 Truncation methods 34

2.13.2 Population control methods 35

2.13.3 Modified sampling methods 35

2.13.4 Partially deterministic methods 36

2.14 Review of Previous Work 36

3 MATERIALS AND METHODS 44

3.1 Introduction 44

3.2 Materials 44

3.2.1 Low-Power Research Reactors 44

3.2.2 Description of the MNSR 46

3.2.3 Physics Design of the MNSR 47

3.2.4 General Description of NIRR-1 48

3.2.5 LEU Dispersion Fuels 51

3.3 Methodology 57

3.3.1 The Monte Carlo Transport Code 57

3.3.2 Monte Carlo Simulation 64

3.3.3 Monte Carlo Estimates 67

3.3.4 NIRR1 MCNP Model 69

3.3.5 Kinetic Parameters of the MNSR 72

3.3.6 Parallel Processing in Monte Carlo 74

4 RESULTS AND DISCUSSION 80

4.1 Fuel Properties 80

4.2 Neutronics Properties 81

4.3 Coefficient of Reactivity 86

4.4 Flux Distribution 89

4.5 Kinetic Parameters 98

4.6 Power Distribution 100

5 SUMMARY, CONCLUSIONS AND RECOMMENDATIONS 102

5.1 Summary and Conclusion 102

REFERENCES 104

LIST OF TABLES

Table 3-1 Characteristics of the NIRR-1 HEU Core 49

Table 3-2 Dimensions of the beryllium reflectors 50

Table 3-3 Elemental Composition of Beryllium reflector 50

Table 3-4 Potential LEU fuels for Research Reactors 55

Table 3-5 MCNP Surface Cards 60

Table 3-6 Types of Tallies available in MCNP 64

Table 3-7 Comparison of PVM and MPI parallel processing methods 75

Table 3-8 System configuration of nodes employed in the study 78

Table 3-9 Job runtime for different parallel computing system configurations 78

Table 4-1 Fuel Material Properties of the Candidate LEU Fuels 81

Table 4-2 Measured and calculated core physics data of reference HEU and candidates LEU fuels 84

Table 4-3 Coefficient of Reactivity 87

Table 4-4 John Stillman's Data Based on CRC Handbook at 1 atm 88

Table 4-5 Calculated thermal, epithermal and fast flux in the inner and outer irradiation sites 91

Table 4-6 Calculated thermal, epithermal and fast flux in the fission chamber and the slant tube 91

Table 4-7 Flux Ratios in the Inner Irradiation Site 92

Table 4-8 Peak flux in the inner irradiation channels in n/cm2.s for HEU and candidate LEU -U3Si 92

Table 4-9 Comparison of kinetics data of LEU fuels with data for the HEU core 99

LIST OF FIGURES

Figure 2-1 Rejection Sampling (Jain 2010) 29

Figure 3-1 Schematic of a Dispersion Fuel 52

Figure 3-2 Monte Carlo Decision Points 66

Figure 3-3 Cross Section of the MNSR Core - Source FSAR(2005) 70

Figure 3-4 MNSR Vertical cross - Source FSAR (2005) 71

Figure 4-1 Dependence of reactivity on Fuel Temperature 88

Figure 4-2 Dependence of reactivity on Moderator Temperature 89

Figure 4-3 Dependence of reactivity on Moderator Density 89

Figure 4-4 Axial thermal flux distribution for HEU and Candidate LEU fuels in the inner and outer irradiation channels 94

Figure 4-5 Thermal flux ratio HEU with candidate LEU fuels in a selected inner irradiation channel 95

Figure 4-6 Comparison of axial thermal, epithermal and fast flux for the HEU and LEU fuels in the inner irradiation channel 96

Figure 4-7 Axial thermal neutron flux distribution as a function of operating power 97

Figure 4-8 Axial Thermal Neutron Flux distribution for different moderator temperatures 98

Figure 4-9 Peak Power Axial Profile 100

Figure 4-10 Comparison of the Power Peaking Factors for HEU core and LEU cores 101

1 INTRODUCTION

1.1 General Introduction

Nuclear research and test reactors worldwide have been in operation for over 60 years, supporting nuclear science and technology development as well as playing an important role as a research tool in scientific fields such as medicine, agriculture, industry and basic research. Parrish *et al*., (2007). Research reactors comprise a wide range of commercial nuclear reactors, which are generally not used for power generation but deployed as a primary source of neutrons in nuclear research activities.

Several benefits are derivable from the use of research reactors even within the constraints of the financial resources of developing countries. These benefits include genetic mutation of seeds leading to seeds differentiation and increased yield. Soil fertility studies benefit from the use of radioisotopes in the understanding of interplay in soil-plant interactions. Radiotracers are in commonplace use in geothermal energy surveys, for the detection of leakages in pipes, dams, and reservoirs. A most relevant application is in Neutron Activation Analysis (NAA).

The acquisition of a reactor facility is a first step in the appreciation of the benefits by providing a medium through which NAA and production of short-lived radioisotopes can be carried out. Research in reactor statics, dynamics and thermal-hydraulics, as well as teaching and training can be performed using such facilities.

In the 1950s and 1960s, research reactors were built using fuel containing U-235 enriched to 20% or less by weight Glaser (2007). However, the expanded use of research reactors in fundamental research, materials testing and radioisotope production created a demand for higher specific power and a need for greater U-235 concentrations, which led to the substitution of the fuel, employed with highly enriched uranium (HEU) reaching at least

70% or even 90%. Muranaka (1983). The HEU fuel, being more economical could be used for a longer period in the reactor core in addition to possessing higher specific reactivity. Owing to the ready availability of the HEU in addition to these other benefits, the HEU fuels were then deployed in both high and low power research reactors.

The use of HEU to fuel research reactors directly lead to a set of inevitable and obvious proliferation risks that are associated with diversion and/or theft of the material. IAEA (1978). Increasing concerns on proliferation and the relative ease of access to the acquisition of nuclear weapons by state and non-state actors led to the initiation of the Reduced Enrichment for Research and Test Reactors (RERTR) program by the US Department of Energy DOE in 1978. The mandate of the program is to develop the technology necessary to convert research reactors and medical isotope production processes to the use of low enriched uranium (LEU) fuel and targets. Since then, there has been an international effort to reduce and eventually eliminate the civil use of HEU. Travelli, (1999).

The RERTR program has identified 106 research and test reactors in the United States and abroad for conversion to LEU fuel. Landers (2005). 42 research and test reactors identified as eligible for conversion to LEU fuel have been fully or partially converted (32 full, 10 partial). The Nigeria Research Reactor-1 (NIRR-1) is one of the 64 Reactors utilizing high U-235 concentrations yet to be converted. Lack of fabrication facilities and capabilities in some countries influence the decision to seek LEU as candidates for replacing fuels in the reactor core.

Due to the need to assure continuity in the supply chain of nuclear fuels in the face of probable restrictions on the sourcing of HEU in the future, the exigency of conversion program of research reactors from the use of HEU to LEU became apparent. This

necessitated the establishment of a Monte Carlo-N Particle Code (MCNP) full core model for the conversion of NIRR-1 facility from the current use of HEU to LEU. Jonah *et al*, (2007).

The MCNP method is a statistical simulation technique whose particle transport capabilities have been employed in many specializations since its introduction in the 1940s. Metropolis (1949) and Verhaegen (2003). Applications of MCNP in Reactor physics design, especially reactor physics parameters, have been discussed in numerous publications Jonah *et al*, (2007, 2009), Khattab and Sulieman (2011) and Abtin *et al* (2013) and have been demonstrated to be an accurate method for reactor design. For neutron transport problems, the Monte Carlo method simulates individual particle tracks by sampling quantities from the probability distributions governing the individual physical processes using machine-generated pseudo-random numbers. X-5 Monte Carlo Team (2003) and tracked through a sufficiently large number of particle histories from which the neutron flux, energy spectrum, and power distribution can be computed.

In addition to neutron transport calculations, the Monte Carlo methods have also been used to simulate particle transport of clinical photon and electron beams Ke *et al* (2009). Reactor design, modeling, and analysis are also routinely carried out using the Monte Carlo methods through the evaluation of k_{eff} in criticality calculations and power and reaction rate distributions - Brown (2009). The MCNP code was developed at the Los Alamos National Laboratory (LANL) for the simulation of neutron transport and the modeling of key reactor parameters from which flux, power distributions, and reaction rates can be calculated. NEA (2006).

Since the inception of the RERTR program in 1978, there has been an intensive effort in the core conversion of varying types of research reactors all over the world.

Previous work includes Mahmood *et al* (2008) in which they established through the deployment of Winfrith improved multigroup scheme (WIMS) and CITATION a reactor code analysis code that a 12.6% UO_2 fuel using Zircaloy-4 clad adequately replaces a 90.2% enriched HEU fuel (UAl4 -Al) from the neutronics point of view. LEU UO_2 has been used in an MNSR type reactor SLOWPOKE-2 in both Jamaica and Canada Kennedy *et al*, (2002). Jonah *et al*, in (2006 and 2009), established thermodynamics and neutronics basis which employed the use of various low enriched UO_2 fuel options. The results indicate that LEU conversion does not adversely affect the neutron flux levels in the irradiation channels.

Khattab and Sulieman (2009) developed a 3D neutronics model for the core conversion of the Syrian MNSR from 89.97% HEU (UAl_4) to 19.75% LEU which yielded core excess reactivity of 5.17mk with 347 HEU fuel rods and 4.85mk with 200 LEU fuel rods respectively

This work model the NIRR-1 using the MCNP for conversion to LEU with three dispersion fuels U_3Si_2, U_3Si and U_9Mo clad in aluminum to determine the core physics parameters, kinetic parameters, neutron flux in the irradiation channels and fuel-pin power distribution.

1.2 Statement of the Problem: HEU, LEU, and Proliferation

Research efforts in the conversion of reactors from HEU to LEU were premised on several factors. The first of which is the proliferation potential of research reactor fuels based on HEU, the concern of which has been heightened in the light of recent developments in some countries where compliance with international regulations and control of nuclear facilities' operations by the IAEA cannot be guaranteed.

Another factor is the need to guarantee the continued availability of nuclear fuels in view of the possible restrictions on HEU fuel supply chain. Countries desirous of the incorporation

of nuclear sources for diversification in power generation are thus better assured of energy security. It is worthy of note that the fabrication of the HEU fuels will be extinct in the future. Bokhari and Pervez (2010).

The reduction in requirements of physical security in the handling of nuclear materials with lower enrichment during fabrication, transportation, usage, and storage is another factor for considering core conversion. The suitability of any candidate material for fueling reactors or even as a fissile material in a nuclear weapon is determined principally by its enrichment, which is the weight fraction of U-235 in the uranium composition.

The use of lower enrichment in any uranium-based fuels is however linked with an increase in the plutonium build-up resulting from neutron capture reaction in U-238, which is another concern in nuclear proliferation. It is thus notable that the search for a suitable fuel material should consider the need for the suppression of this plutonium buildup. Studies have shown that below certain enrichment value set at 20%, the design and construction of any nuclear weapon or an explosive device becomes an unrealistic venture. This is due to the fact that at less than 20% enrichment, LEU is not attractive as a gun-type device owing to its large critical mass and neutron emission rate. Fortuitously, at an enrichment value less than 20%, plutonium buildup is suppressed adequately to satisfy the concerns of nuclear proliferation. Thus, the limit set at 20% enrichment provides an optimum target in the process for conversion of research reactors.

1.3 Purpose of this Study

The principal purpose of this study is to perform the core calculations required to convert the NIRR-1 MNSR from HEU to LEU by means of qualified dispersion nuclear fuels in line with current international efforts to reduce global threats from nuclear proliferation. The search for potential LEU options would be constrained by the need to ensure minimal

modifications to the reactor core while maintaining already established safety margins, operational utilization characteristics and fuel reliability of the current HEU core.

1.4 Significance of the Study

This study is a component of the concerted effort of the International Community through the Reduced Enrichment for Research and Test Reactor (RERTR) Program by aiming to minimize the use of highly enriched uranium in civil nuclear applications through its replacement with LEU fuels. The RERTR was initiated in1978 by the US's Department of Energy and has been incorporated into the Global Threat Reduction Initiative (GTRI) established in 2004 at the US Office of Defense Nuclear Nonproliferation and whose mandate it is to facilitate the disposition and reduction of, and offer protection to nuclear and radiological materials in civilian facilities throughout the world.

1.5 Research Aims and Objectives

The aim of this research is to perform the neutronics analyses in support of the conversion of NIRR-1 from UAl_4 HEU fuel to LEU using three dispersion fuels U_3Si_2, U_3Si and U_9Mo clad in aluminum. The objective of this work include:

a) Modeling NIRR-1 Core with U_3Si_2-Al, U_3Si-Al, and U_9Mo-Al LEU dispersion fuels.

b) Optimizing calculations for uranium densities and uranium enrichments that would give sufficient excess reactivity as the current HEU core.

c) Conducting neutronics safety analysis to ensure that margins are as obtained in the existing HEU core with the use of U_3Si_2-Al, U_3Si-Al, and U_9Mo-Al LEU fuels.

2 LITERATURE REVIEW/THEORETICAL FRAMEWORK

2.1 Interactions of Neutron with Matter

The physics of nuclear reactors is dependent on the transport of neutrons in the materials of the reactors and the mechanism of neutron interactions. Owing to neutron charge neutrality, neutrons are not affected by the Coulomb force and are thus able to travel through a few centimetres of material before interacting with other particles. The interaction of neutrons is by physical collisions with the target nuclei which may result in three types of interactions: - compound nucleus formation, potential scattering, and direct interaction.

2.1.1 Compound Nucleus Formation

A compound nucleus is formed because of absorption of an incident neutron in a target nucleus ${}_{Z}^{A}X$ in which the kinetic energy of the neutron E is shared by the nucleons of the nucleus hence leaving the compound nucleus $\left({}_{Z}^{(A+1)}X\right)^{*}$ in an excited state of energy E^{*}.

$$ {}_{Z}^{A}X + {}_{0}^{1}n \rightarrow \left({}_{Z}^{A+1}X\right)^{*} \qquad 2.1 $$

The excited energy of the compound nucleus is larger than incident kinetic energy owing to the contribution of binding energy to the compound nucleus. The compound nucleus being unstable survives for about 10^{-14}s before de-excitation via the following pathways: -

In a resonant elastic scattering, the excited compound nucleus de-excites by expelling a neutron and leaving the target nucleus in the ground state. In an inelastic resonant scattering the residual nucleus is left in an excited state and the energy of the emitted neutron is lower that incident neutron's energy. The excited state may later de-excite by emitting a photon.

An important reaction in reactor analysis is radiative capture as this affect the neutron population. In a radiative capture (n, γ), the compound nucleus de-excites by emitting a gamma ray photon and the nucleus is eventually left in the ground state.

$$ {}^{A}_{Z}X + {}^{1}_{0}n \rightarrow \left({}^{A+1}_{Z}X\right)^{*} \rightarrow {}^{A+1}_{Z}X + \gamma \qquad 2.2 $$

If the resulting nuclide is radioactive, the lopsided neutron-proton ratio in the nuclear stability curve caused by the capture of incident neutron may lead to further beta decay.

The cross-section in capture or absorption reactions is strongly dependent on the speed of the incident neutrons and exhibits resonances for combined neutron energy and binding energy of neutron matching a compound nucleus energy level. The cross-section for neutron interactions involving compound nucleus formation is expressed as the product of the cross-section for the formation of the compound nucleus and the probability of decay via a selected de-excitation pathway. For instance, the cross-section in which a compound neutron de-excites by the emission of an elastic neutron at energy E_c may be written as

$$ \sigma_s(E_c) = \sigma_{CN}(E_c)\frac{\Gamma_n}{\Gamma} \qquad 2.3 $$

Where σ_{CN} is the cross-section for the formation of a compound nucleus and may be expressed near a well-defined and isolated resonance at energy E_1 by the Breit-Wigner single-level formula as

$$ \sigma_{CN}(E_c) = \frac{K}{(E_c - E_1)^2 + \Gamma^2/_4} \qquad 2.4 $$

and Γ_n is the probability of decay by neutron emission and Γ represent the total probability for the decay of an excited state. Lamarsh (1972)

If the compound nucleus decays by the emission of more than one neutrons, may we have (n, 2n), or (n, 3n) reactions, these reactions are increasingly less significant in nuclear

reactor operations and neutron economy as the reaction threshold is greater than the energy of most neutrons available in a reactor.

2.1.2 Potential scattering

Potential scattering is a type of elastic scattering which occurs because of the proximity of neutron to a nucleus occasioned by neutron-nuclei forces which depend on the size and shape of the nuclei. This scattering reaction does not involve a compound nucleus formation but occurs for an incident neutron of any energy and the total energy is conserved in a potential scattering. The kinetic energy E' of the neutron after scattering E' is between $\alpha E \leq E' \leq E$ where E is the incident neutron energy, A is the mass number of the nuclei and $\alpha \approx \left(\frac{A-1}{A+1}\right)^2$ Rozon (1998). This is the basis for neutron moderation in media.

2.1.3 Direct interaction

In this case, a direct collision between neutrons of high energy and a target nucleus leads to the capture of the incident neutron with an ejection of one or more nucleons. If a proton is ejected, we have a direct interaction (n,p) reaction. A direct inelastic scattering occurs if a neutron strikes a nucleon into an excited leading to the ejection of neutron of lower energy. This type of interaction is not of interest in reactor physics as very few neutrons possess such sufficiently high energies.

2.2 Fission neutrons

A compound nucleus formed because of absorption of neutron may decay via fission which is the splitting of the compound nucleus into two lighter nuclei known as fission fragments, secondary neutrons and with the release of energy.

$$^{235}_{92}U + {}^{1}_{0}n \rightarrow \left(^{236}_{92}U\right)^{*} \rightarrow \left\{^{95}_{36}Kr + {}^{139}_{56}Ba\right\} + 2(^{1}_{0}n) + \gamma \qquad 2.5$$

Fission neutrons are produced with a wide range of energies and may be classified into two categories, prompt neutrons which are neutrons released within 10^{-14}s of the fission event and constitutes about 99% of total fission neutrons, some neutrons referred to as delayed neutrons continue to be emitted over a period from beta decay of fission fragments known as delayed neutron precursors. The emission of a delayed neutron by a precursor is possible when the maximum available energy to the beta particle exceeds the binding energy of the neutron in the resulting nucleus. Despite the small fraction of neutrons released as delayed, the presence of these delayed neutrons is crucial for reactor control because their presence provides a long time constant slowing down the dynamic response of the reactor. In addition, the delayed neutrons are produced with a lower energy in comparison to prompt neutrons and are better able to survive leakage and resonance absorption and thus contribute to the neutron dynamics.

Despite the large number of fission products which may decay by neutron emission, we can categorize these delayed neutron precursors into six groups with each i^{th} group characterized by its approximate half-lives or decay constant λ_i and the relative yield fraction $\beta i/\beta$, with each group consisting of different isotopes. Stacey (2001)

2.3 The Multiplication Factor

The presence of neutrons in a fissionable material may lead to new fission because of fission, however, not all neutrons absorbed or captured lead to subsequent fission due to absorption in non-fissionable materials, parasitic absorptions in fissionable material and leakage. A steady-state chain reaction is possible if on the average, at least one neutron produced in fission leads to a subsequent fission in another nucleus. For an infinite medium in which there is no neutron leakage and all neutrons are eventually absorbed and the neutron flux is steady, we may define an important quantity in nuclear design calculations

characterizing the chain reaction in the medium as the infinite multiplication factor, k_∞ being the ratio of the neutrons produced from fission in one generation to the neutrons absorbed in the preceding generation.

When the ratio k_∞, the number of fission in each succeeding generation is constant and the system is termed as critical, for $k_\infty > 1$, the chain reaction diverges and the system is said to be in super-critical state while for $k_\infty < 1$, there is a decrease in the neutron population from generation to generation and the system is termed as sub-critical.

2.3.1 The four-factor formula

Fission neutrons are typically born fast and can interact with surrounding materials via several reaction pathways, some of which leads to a reduction the neutron population via non-fission absorption in nuclear materials, other reactions such as fission and (n,2n) lead to an increase in the neutron population. The infinite multiplication factor is determined by tracing a group of newly born fast neutrons over one generation through the possible reaction channels and is represented by the four-factor formula: -

$$k_\infty = \varepsilon p f \eta \qquad 2.6$$

where ε, the fast fission factor, is defined as the ratio of the net number of fast neutrons produced by all fissions to the number of fast neutrons produced by thermal fission. The resonance escape probability p gives the ratio of the number of neutrons reaching thermal energies to the number of fast neutrons that commence the slowing down process.

The thermal utilization factor f expresses the ratio of the thermal neutrons absorbed in the fuel to the number of thermal neutrons absorbed in all reactor material while the reproduction factor η is defined as the ratio of the number of fast neutrons that are produced by thermal fission to the number of thermal neutrons absorbed in the fuel.

For a real, finite reactor, it is necessary to include the probability of neutron leakage by expressing the effective multiplication factor k_{eff} as the ratio of the neutrons produced by fission on one generation to the cumulative number of neutrons lost through absorption and leakage in the preceding generation.

The effective multiplication factor can be expressed in terms of the infinite multiplication factor by

$$k_{eff} = k_{\infty} P_{nl} \qquad 2.7$$

where P_{nl} known as total non-leakage probability measures the probability that neutrons would not be leaked out of the system before absorption.

2.3.2 The six-factor formula

Neutron leakage may be classified into two categories, that which occurs during the slowing down process and that which occurs after the neutrons have reached thermal energies. Hence, we may express P_{fnl} (fast non-leakage) as the probability that fast neutrons would not leak out of the system and P_{tnl} (thermal non-leakage) as the probability that thermal neutrons would not leak out yielding the six-factor formula containing all the factors characterizing the neutron life-cycle

$$k_{eff} = \varepsilon p f \eta P_{fnl} P_{tnl} \qquad 2.8$$

The parameters in the four-factor formula depend strictly on the material of the reactor while the two non-leakage probabilities are functions of the size and the shape of the reactor. Change in the reactivity of an MNSR reactor is achievable by altering the thermal utilization factor. The non-leakage probability is affected by the presence of a reflector material in the reactor. Fast fission factor is essential determined by the core configuration while the resonance escape probability is affected by the fuel enrichment and the fuel-

moderator arrangement. The reproduction factor is strictly dependent on the fuel enrichment. It is to be noted that the last three factors are not easily altered in the MNSR.

2.4 Reactivity

Reactivity is a measure of departure of a reactor from criticality and is represented by a dimensionless quantity ρ as given below

$$\rho = \frac{k_{eff} - 1}{k_{eff}} \qquad 2.9$$

where k_{eff} is the effective multiplication. Hence for a critical assembly where k_{eff} is 1, reactivity is 0, while for a subcritical system, $k_{eff} < 1 \; thus \; \rho < 0$, and for a supercritical assembly, $k_{eff} > 1, and \; \rho > 0$. Common units for expressing reactivity in research reactors include cents and dollars, pcm or %Δk/k and represent a departure from prompt criticality conditions.

2.4.1 Control of reactivity

In reactor operations efforts is made to ensure a steady state in which reactivity is 0. At the startup of the reactor, a positive reactivity is inserted gradually for a short period to attain the desired power level. At shut down, or when a lower power level is required, a negative reactivity is inserted using a reactor control rod made of strong neutron absorbers such as cadmium or boron.

To compensate for changes in reactivity because of fuel burn up and negative reactivity feedback caused by an increase in temperature, reactor cores are designed with an initial core excess reactivity using a core loading and enrichment to guarantee power operation for an optimum period. It becomes necessary to have a means of controlling for this excess

reactivity through the introduction of negative reactivity which can be controlled at will to allow for reactor operation at determined power levels. In the MNSR NIRR-1, a small cadmium material was inserted in one of the irradiation channels to bring the core excess reactivity to conform to the design basis. FSAR (2005), Jonah *et al* (2007)

2.4.2 Coefficients of reactivity

A reactivity coefficient is defined as the change in reactivity as a function of change on some property of the system, such as fuel temperature, moderator temperature, and the moderator density or void fraction Dawahra *et al* (2016). For example, the moderator temperature coefficient of reactivity α_T may be defined as

$$\alpha_T = \frac{d\rho}{dT} = \frac{1}{k^2_{eff}} \frac{dk_{eff}}{dT} \approx \frac{1}{k_{eff}} \frac{\Delta k_{eff}}{\Delta T} \qquad 2.10$$

where k_{eff} is the effective multiplication factor, T is the moderator temperature and ρ is the reactivity.

For safety consideration, the core of the MNSR is designed to be under-moderated meaning that a reduction or removal of coolant reinforces safety by causing a decrease in reactivity thus self-regulating.

2.5 Boltzmann Equation

The neutron transport equation is a linearized form of the Boltzmann transport equation which describes the distribution of neutrons as a function of space coordinates, energy and time in each volume. It expresses the principle of neutron conservation of neutron balance and it takes into consideration scattering, absorption, leakages, neutron production in addition to external sources of neutrons. The knowledge of the neutron distribution function is sufficient to solve almost all problems of interest in reactor theory;

The neutron balance equation in terms of the angular neutron density with seven

independent variables of *r(x, y, z), E, Ω(θ,ϕ) and t* given by Duderstadt and Hamilton (1976) is

$$\frac{\partial n}{\partial t} + v\hat{\Omega}\cdot\nabla n + v\Sigma_t n(\vec{r},E,\hat{\Omega},t) = \int_{4\pi} d\hat{\Omega}\int_0^{\infty} dE' v'\Sigma_s\left(E'\to E,\hat{\Omega'}\to\hat{\Omega}\right)\mathrm{n}\left(\vec{\mathrm{r}},\mathrm{E}',\hat{\Omega}',t\right) - s(\vec{r},E,\hat{\Omega},t) \qquad 2.11$$

where $n(\vec{r},E,\hat{\Omega},t)d^3rdEd\hat{\Omega}$ is the expected number of neutrons in d^3r about $\vec{r}$, energy dE about E, moving in the direction $\hat{\Omega}$ in solid angle $d\hat{\Omega}$ at time t. The source term $s(\vec{r},E,\hat{\Omega},t)d^3\vec{r}dEd\hat{\Omega}$ represents the rate of sources of neutrons appearing in the volume d^3r about $\vec{r}$, energy dE about E, moving in the direction $\hat{\Omega}$ in solid angle $d\hat{\Omega}$. The net leakage of neutrons through the surface is given by $v\hat{\Omega}\cdot\nabla n$, while the losses due to collisions in volume V is represented by $v\Sigma_t n(\vec{\mathrm{r}},E,\hat{\Omega},t)$ and gain because of in scattering of neutron into energy dE about E, moving in the direction $\hat{\Omega}$ in solid angle $d\hat{\Omega}$ from other energies and directions is given by

$$\int_{4\pi} d\hat{\Omega}\int_0^{\infty} dE' v'\Sigma_s\left(E'\to E,\hat{\Omega'}\to\hat{\Omega}\right)\mathrm{n}\left(\vec{\mathrm{r}},\mathrm{E}',\hat{\Omega}',t\right) \qquad 2.12$$

Expressing the equation in terms of the angular neutron flux and differentiating between neutrons produced from fission and external sources of neutrons and re-arranging the terms, we have: -

$$\begin{aligned}\frac{1}{v}\frac{\partial\psi(\vec{r},E,\hat{\Omega},t)}{\partial t} &= Q(\vec{r},E,\hat{\Omega},t) + \iint \psi\left(\vec{r},\acute{E},\hat{\Omega}',t\right)\Sigma_s\left(\vec{r},\acute{E}\to E,\hat{\Omega}'\to\hat{\Omega}\right)d\hat{\Omega}'dE' \\ &+ \frac{\chi(\vec{r},E)}{4\pi}\iint v\Sigma_f(\vec{r},E)\psi\left(\vec{r},\acute{E},\hat{\Omega}',t\right)d\hat{\Omega}'dE' \\ &- [\hat{\Omega}\cdot\nabla + \Sigma_t(\vec{r},\acute{E})].\psi\left(\vec{r},\acute{E},\hat{\Omega}',t\right)\end{aligned} \qquad 2.13$$

which may be abbreviated as

$$\frac{1}{v}\frac{\partial\psi(\vec{r},E,\widehat{\Omega},t)}{\partial t} = Q + [S+M]\cdot\psi - [L+T]\cdot\psi \qquad 2.14$$

Where L is the leakage operator, M is the fission multiplier, T is the collision operator and S is the scattering operator. Hence $[S+M]$ represents the gains term from scattering and neutron multiplication while $[L+T]$ represents losses from leakages and collisions.

Owing to the dependence of macroscopic cross-sections on position due to the non-uniform structure of reactor cores and the complicated dependence of cross-section as a function of energies especially in the resonance region, the solution of the linear neutron transport equation is quite convoluted, except in very simple but unrealistic cases, hence the resort to some approximation methods.

One approach at solving the transport equation is by discretizing i.e. replacing the functions of continuous variables by a discrete set of values at enumerated points by means of the following methods: - the discrete ordinates S_n methods or the function expansion P_n methods. Duderstadt and Hamilton (1976).

Discretizing the energy variable using the discrete ordinate method where the neutron energy of interest is divided into a finite number of groups in which the cross-section representing each group is constant and evaluated as the average cross-section over energy and is independent of position leads the multi-group S_n method. Bell and Glasstone (1970).

A common approximation method is the one-speed neutron diffusion theory in which the neutrons are assumed to have one effective speed and neutrons are scattered from a nucleus of infinite mass, hence there is no neutron energy loss. Using the Fick's law which states that J, the current density is approximately the negative spatial density of the flux ϕ i.e.

$$J(\vec{r},t) \approx -D(r)\nabla\phi(\vec{r},t)$$

where *D* is the diffusion coefficient.

The neutron transport equation reduces to the much simpler one-speed neutron diffusion equation. Duderstadt and Hamilton (1976)

$$\frac{1}{v}\frac{\partial \phi}{\partial t} = \nabla \cdot D(\vec{r})\nabla\phi - \Sigma_s(r)\phi(\vec{r},t) + S(\vec{r},t) \qquad 2.15$$

It is noteworthy to state that the diffusion approximation represented in Fick's law is valid under the assumptions: -

i. That absorption reaction is much less likely to occur than scattering,
ii. that the spatial variation in neutron distribution is linear
iii. and the neutron scattering is isotropic.

This first requirement is satisfied in most water moderated reactors. Within a few mean free paths from the boundary of homogeneous media, we may consider neutron source to be uniform and assume that scattering from heavy atomic mass nuclei to be isotropic.

The approaches considered so far for the solution of the Boltzmann's transport equation are classified as deterministic method as they attempt to solve the neutron transport equation for an average behavior of the particles. A different approach is the Monte Carlo method which is a numerical approach that is based on statistical theory and whose underpinning is that the macroscopic cross-section for a reaction may be considered as the probability of interaction per unit distance traversed by a neutron. In the Monte Carlo method a batch of neutron histories is generated by tracking each neutron through successive interactions involving scattering, radiative capture, and fission, the nature of each interaction and the resulting direction and energy of the resulting neutron is simulated by means of random number sets from which the aggregate characteristics of the system is determined.

Glasstone and Sesonske (2004). The applicability of the Monte Carlo method is the possibility of simulating sequentially individual particles of a system since the physical events and interactions are not correlated. Glaser (2005)

2.5.1 Integral form of the Boltzmann equation

While deterministic discrete ordinates method is said to solve the integro-differential neutron transport equation, the Monte Caro method provides a solution to the equivalent integral transport equation obtained by introducing in equation 2.13 an integration factor

$$exp\left[-\int_0^R \Sigma_T(\vec{r} - R\,\widehat{\Omega}, E)dR\right] \text{ where } R\widehat{\Omega} = \vec{r} - \vec{r}'$$

If we define $\vec{E} = E \cdot \widehat{\Omega}$

Collision density as $\Psi(\vec{r}, \vec{E}) = \Sigma(\vec{r}, E) \cdot \psi(\vec{r}, \vec{E})$ and

Transport kernel as $T(\vec{r}' \to \vec{r}, \vec{E}) = \Sigma_T(\vec{r}, E).exp\left[-\int_0^{|\vec{r}-\vec{r}'|} \Sigma_T(\vec{r}' + s\widehat{\Omega}, E)ds\right] \cdot \frac{\delta(\Omega \cdot \frac{\vec{r}-\vec{r}'}{|\vec{r}-\vec{r}'|} - 1)}{|\vec{r}-\vec{r}'|^2}$

and the Collision kernel as $C(\vec{E}' - E, \vec{r}) = \frac{\Sigma_S(\vec{r}, \vec{E}' \to \vec{E})}{\Sigma_T(\vec{r}, E')} + \frac{\chi(\vec{r}, E)\nu\Sigma_F(\vec{r}, E')}{4\pi \cdot \Sigma_T(\vec{r}, E')}$ which yields the integral form of the transport equation. Irving (1971), Dunn and Shultis (2012)

$$\Psi(\vec{r}, \vec{E}) = \int \left[\int \Psi(\vec{r}', \vec{E}').C(\vec{E}' \to \vec{E}, \vec{r})d\vec{E}' + Q(r, E)\right] \cdot T(\vec{r}' \to \vec{r}, \vec{E}')\,d\vec{r}' \qquad 2.16$$

2.6 Neutron Cross Section Data Libraries

In Monte Carlo transport problems, the quality of the output is strongly dependent on the accuracy of the geometry representation, the statistical uncertainty in the Monte Carlo computation and the nature of the neutron and photon interactions as presented in the cross-section data. The nature of the MCNP problem under consideration determines the specification o the cross-section and the data source available to the user. While cross-section data may be presented for an element that occurs in nature as a single isotopic

value, in photonuclear reactions, the cross-section for each isotope would need to be provided for accuracy.

The cross-section data consists of the neutron-nuclei interactions, the interaction of photons with nuclei and the production of photons from neutron-nuclei interaction. An analysis of experimentally measured cross-section data combined with predictions from nuclear model calculation gives a more accurate representation of the interactions and is referred to as an Evaluated Nuclear Data File (ENDF). Significant discrepancies have been reported in the results calculated using cross-section libraries based on different evaluated nuclear data files, hence it is important to take into to consideration a benchmark to validate the ENDF source. Since the MNCP cannot directly use evaluated data in ENDF format, it is pre-processed into the A Compact ENDF (ACE) format using the NJOY code for ENDF-5 and ENDF6 format and the MCPOINT code for ENDL formats. Little and Seamon (1985)

The continuous-energy cross-section data contains all cross-section data on a fixed main energy grid which is close enough to allow for linear interpolation between energy points and can reproduce cross-section data to a tolerance of about 1%.

In a bid to optimize data storage for MCNP computation on small systems, discrete reaction tables, the cross-sections are averaged into 262 groups using a flat weighting function and presented in the form of histograms as against the continuous curves.

In this work, the neutron interaction for both the continuous-energy and discrete reaction data are presented using the XSDIR file containing entries for each isotope and selected via a unique identifier known as ZAID where Z is the atomic number and A is the mass number. Cross-section data for all materials present in the core are included in the simulation.

2.6.1 Thermal neutron scattering

The MCNP code assumes that for neutrons of thermal energy, motion of scattering nuclei may be described by the free gas model, however, most scattering nuclei would exist in form of molecules bound in either solid or liquid form, which thus affects the nature of the interaction between the free neutron and the scattering nuclei through excitation in the nuclei hence causing a change in the reaction cross-section. This effect is important for neutrons of energy <= 4eV interacting with nuclei and is strongly affected by temperature. Scattering of neutrons by a system of particles is characterized by contributions from coherent scattering and incoherent scattering terms which in turn is made up of elastic and inelastic parts.

It is customary to divide thermal scattering cross-section into three parts: - coherent elastic (which is significant for crystalline solids such as graphite), incoherent elastic (important in hydrogenous materials and inelastic scattering for all materials.

In crystalline solids, the coherent elastic differential scattering cross section is given by

$$\sigma_{coherent}(E,\mu) = \frac{\sigma_c}{E}\sum_{E_i<E} f_i e^{-4WE_i}\,\delta(\mu-\mu_i) \qquad 2.17$$

MacFarlane et al, (2012), where μ is the cosine of the scattering angle, $\mu_i = 1 - {}^{E_i}/_{E}$ and

E_i are the Bragg edges, σ_c is the effective bound coherent scattering cross-section and f_i is obtained from crystallographic structure factors.

while incoherent elastic scattering is the component of the scattering term from zero phonons and is given by

$$\sigma_{incoherent}(E,\mu) = \frac{\sigma_b}{2} e^{-2W(1-\mu)} \qquad 2.18$$

where W is the Debye-Waller coefficient denoted by $W = \frac{\lambda}{AkT}$ and is dependent on the input frequency and temperature T, σ_b is the characteristic bound cross-section and the energy grid of the elastic cross-section is E

The double scattering cross-section contribution from inelastic scattering for thermal neutrons in gases, liquids or solids as presented by MacFarlane et al, (2012), is

$$\sigma(E \to \acute{E}, \mu) = \frac{\sigma_b}{4\pi T}\sqrt{\frac{\acute{E}}{E}}e^{-\frac{\beta}{2}}S(\alpha,\beta) \qquad 2.19$$

where S(α,β) is the asymmetric scattering law, $\propto = \frac{\acute{E}+E-2\mu\sqrt{E\acute{E}}}{AkT}$ and $\beta = \frac{\acute{E}-E}{kT}$ are dimensionless momentum and energy transfer parameters respectively. A is the ratio of the scattering nuclei mass to the mass of the neutron, E and E′ are the incident and final neutron energies, σ_b is the bound scattering cross-section for the material of interest.

For free gas scattering target such as gases and unbound nuclei, S(α,β) may be given by

$$S(\alpha,\beta) = \frac{1}{4\pi\alpha}\exp\left(-\frac{\alpha^2+\beta^2}{4\alpha}\right) \qquad 2.20$$

The S(α,β) scattering laws into takes account the binding of effects of nuclei and are described in the Evaluated Nuclear Data file ENDF. Trellue and Little (2008). ENDF is processed using the NJOY code for use in the MCNP and is represented in the input file by means of the MTn card associated with an existing material card Mn. The data is available in the MCNP libraries for materials such as water, heavy water, polyethylene, methane, graphite, beryllium, zirconium-hydride, etc.

2.7 The History of the Monte Carlo Method

One of the earliest instances of the application of random sampling towards the solution of problems was by Comte de Buffo (1707-1788) in which he attempted the use of repeated tosses of a needle onto a lined background to estimate the value of pi from the probability of the needle intersecting the lines. Kalos and Whitlock (2008). A similar application was conducted by Lord Kelvin in evaluating some time integrals of kinetic energy in his studies of the kinetic theory of gases. Kelvin (1901). The late nineteenth and early twentieth century witnessed works by E. L. Forest, G. H. Darwin and W.S. Gosset where simulation was increasingly employed as an experimental method for confirming the theory and analyzing data.

Following the discovery of the neutron in the 1930s, Enrico Fermi conducted some numerical experiments in what would nowadays be considered as a Monte Carlo calculation to estimate how the newly discovered neutron would interact with condensed matter. Dunn and Shultis (2012).

During the Second World War, the Manhattan research project brought together scientists such as Fermi, von Neumann, Ulam, and Metropolis and with the advent of digital computers, accelerated the application of the Monte Carlo methods in areas such as radiation transport, statistical mechanics, properties of neutron travel through radiation shielding materials. Anderson (1986)

Von Neumann and Ulam refined the direct simulation method using variance-reduction techniques such as Russian Roulette and splitting methods. Fermi, Metropolis, and Ulam in 1948 obtained Monte Carlo estimates of the eigenvalues of Schrodinger's equation. Hammersley and Handscomb (1964)

One of the first actual Monte Carlo calculations was carried out on the ENIAC computer in form of the Metropolis algorithm for investigating equations of state for substances consisting of interacting individual molecules through the modification of Monte Carlo integration over configuration space. Metropolis *et al* (1953)

The Monte Carlo method is now a veritable tool deployed for complex problems that are intractable analytically, impractical, costly or time-consuming to be conducted experimentally. The solution of such problems often involves huge computing resources but techniques exist to optimize resource requirements while preserving accuracy.

The Monte Carlo method for particle transport is the principal tool used in this work and it involves the simulation and tracking of the particles from birth through interactions such as absorption or leakage out of the system. The nature and frequency of the interactions is randomly sampled according to the probability distribution functions guided by the appropriate physical laws.

2.8 Monte Carlo and Criticality Calculations

One method of solving the linear Boltzmann transport equation for neutrons is by a Monte Carlo simulation approach whereby particles are tracked through the system and by assuming the following: -

- Each neutron history is considered as independent and identically distributed
- The probability density for all neutrons is the same throughout the phase space, and
- The geometry and material composition do not change within the solution interval of interest.

As the neutron traverses the materials, it interacts with the constituent atoms undergoing elastic scattering, fission, and absorption, the probability of which is determined by the

cross-sections. Despite the stochastic nature of the interactions, it is possible to determine the distribution of flight paths of a large number of interacting particles by means of random walk analysis. The analysis would indicate results such as the secondary directions of neutron following a scattering interaction, the number of neutrons created from fission etc. thus producing a lifecycle of neutrons from birth to absorption or leakage out of the system. The various events during the lifecycle are then tabulated and reported as the history for that particle.

If we assume that there is no external neutron source we may re-write Eq 2.14 the time-independent Boltzmann equation as

$$[L+T]\psi_k(\vec{r},E,\widehat{\Omega}) = [S+\frac{1}{k_{eff}}M]\psi_k \qquad 2.21$$

Where a scaling factor k_{eff} effective multiplication factor has been introduced in place ofν yielding a steady-state static eigenvalue equation problem in $\psi_k and\ k_{eff}$.

Rearranging Eq. 2.21 gives

$$(L+T-S)\psi_k = \frac{1}{k_{eff}}M\psi_k \qquad 2.22$$

Hence

$$\psi_k = \frac{1}{k_{eff}}\cdot(L+T-S)^{-1}M\psi_k \qquad 2.23$$

Eq. 2.22 may be solved numerically using the standard power iteration method. X-5 Monte Carlo Team (2003) by making an initial guess for the $\psi_0 and\ k_{eff}$ where each iteration cycle corresponds to a single fission generation. With a given fission neutron source distribution and an estimate of the effective multiplication factor, single random walks are

conducted for a batch of neutrons to determine the next iteration by following the particle history and solving for ψ^{n+1}. The sites where fission occurs are saved to be used as sources in the next iteration.

An estimate of the effective multiplication factor is obtained using

$$k_{eff}^{n+1} = k_{eff}^{n} \frac{\int M\, \varphi^{n+1} d\vec{r}}{\int M\, \varphi^{n} d\vec{r}} \qquad 2.24$$

The procedure is then repeated till convergence occurs, and the iteration continues for the computation of the tallies of k_{eff} and reaction rate. The is an initial guess for k_{eff} and estimate of convergence represented in the MCNP code by the KCODE card.

2.9 Mathematical Basis for Monte Carlo Simulation

2.9.1 Generation of random numbers

Random numbers are commonly used in Monte Carlo methods to aid in the simulation of stochastic processes representing a variable changing randomly with time or in complex problems where analytic solutions are either unavailable or the problems in impracticable or dangerous to undertake and as such a stochastic approach is preferable to a deterministic method. A most commonly cited source of a true random number generator is that of a material undergoing radioactive decay where the substance transmutes into another at random points in time.

Owing to the impracticability of generating random numbers from truly random external sources, the random numbers sources used in statistical simulations are generated from deterministic algorithms on digital computers and are classed as pseudorandom numbers with a period capable of reproducing a stream of numbers that may be characterized as truly random. Several publications have recommended the use of quasi-random numbers

for complex problems. These numbers are defined as low discrepancy sequences which offer improved asymptotic convergences rates than pseudorandom numbers. Azmy and Sartori (2010)

A uniform distribution of pseudorandom numbers can be produced by the linear congruency generator proposed by Lehmer (1951) given by

$$x_{i+1} = (ax_i + c)\ mod\ m\ for\ i \geq 0 \qquad 2.25$$

The multiplier a > 1, the increment c and the modulus m is carefully chosen and the initial value of x is x_0 known as the seed. The output is a sequence of random numbers in the range of $(0 \leq x_i \leq m)$ which is then scaled to the interval [0,1] by dividing by m.

One of the characteristics that a good random number generator must possess is that of a long period, portability, efficiency. It must also pass the statistical tests for randomness such as the diehard test. Marsaglia (1985).

Most random number generators in MCNP and other Monte Carlo codes for particle transport employ algorithms based on the linear congruential generators (LCG). The form of the LCG used in the MCNP code. Brown (2007) is

$$S_{k+1} = kS_k + c \cdot mod\ 2^M \qquad 2.26$$

and

$$r_{k+1} = {S_{k+1}}/{2^M} \qquad 2.27$$

Which generates output in the interval [0,1] and S_k, g and c are integers that are expressible in M bits or fewer and r_{k+1} is a floating-point number. The seed value of S_k generator is S_0, if c = 0 and g mod 8 = 3 or 5, then the period of the generator id 2^{M-2}, for c not equal to zero and odd, then the period is 2^M. The traditional linear generator uses the following values of $\{g = 5^{19}, c = 0, S_0 = 5^{19}, M = 48\}$

Large Monte Carlo calculation often involves the use of a billion or more particles histories, so to avoid the reuse of random numbers, the algorithm has been extended to use 63 bits thus giving a period of 2^{63}.

The Random Number Generator (RNG) employed in the MCNP code satisfies the following criteria, some of which are that the sequence of numbers produced are deterministic to guarantee repeatability if experiments, the initialization of the RNG is simple and state information to specify the history is minimal. The linear congruential generator algorithm uses only a small number of arithmetic operations to speed up the calculations.

2.9.2 Probability density function

Let us consider a single continuous variable defined over a finite or an infinite interval as x, then we may denote the probability that the observed value of x_i <= X is given by

$$Prob\{x_i \leq X\} \tag{2.28}$$

The probability density function (PDF), f(x) has the following characteristics, it must be a non-negative real-valued function, it is defined on the interval of interest [a, b] where b > a and it is normalized such that the integral over the range is 1. i.e.

$$\int_a^b f(x)dx = 1 \tag{2.29}$$

f(x)dx gives the probability that a random sample would yield the value x about dx and is represented as

$$f(x)dx = Prob\{x \leq x_i \leq x + dx\} \tag{2.30}$$

2.9.3 Cumulative distribution function

The cumulative distribution function (CDF) represented by $F(x_i)$ gives the probability that a random sampling of variable x would take a value less than or equal to x_i i.e.

$$F(x_i) = Prob\{a \leq x \leq x_i\} \quad 2.31$$

2.10 Sampling Methods

Monte Carlo simulations typically involve the sampling of random events representing the behavior of the phenomena under study, thus giving a probability distribution f(x), a sampling process yields a sequence of values closely mimicking the original distribution.

2.10.1 Inverse CDF method – continuous distribution

Let a random variable x be represented by a probability distribution function f(x) and a cumulative distribution function F(x). Since CDFs are monotone increasing functions with values between [0,1], then there exists an inverse function F^{-1} with values between [0,1] such that

$$F^{-1}(y) = \min\{x: F(x) \geq y\} \quad 2.32$$

$$\text{for } y \in [0,1]$$

with sampling points that follows the original PDF. The method is efficient for generating samples of random variables for distributions for which the inverse CDF value is known.

2.10.2 Inverse CDF method – discrete distribution

Assume that random variable x can take on discrete values of x_i with probability f_i, then we may write probability density and cumulative distribution function as

$$f(x) = \sum_{i=1}^{N} f_i \, \delta(x - x_i) \quad 2.33$$

$$\text{and } F(x) = \sum_{x_i \leq x} f_i$$

To generate values of x with this CDF, we select random number u uniformly distributed between 0 and 1 and find number xi satisfying $F(x_{i-1}) < u \leq F(x_i)$ using the following method

a. Pick a random u between 0 and 1

b. Set *i*=1

c. If $u \leq F(x_i)$, then return x_i, else increment *i* and repeat step c

2.10.3 Acceptance-rejection method

An explicit formula representing the inverse CDF function of a random variable may not always be possible. A more efficient method for complicated distribution is the acceptance-rejection method first proposed by Neumann. In **Figure 2-1** let *p(x)*represent the real distribution of variable *x* and *M.q(x)*some other scaled distribution such that *q(x) > 0* for all *p(x) >0,* where M is a constant multiplier such that *p(x) <= M.q(x)*for all x.

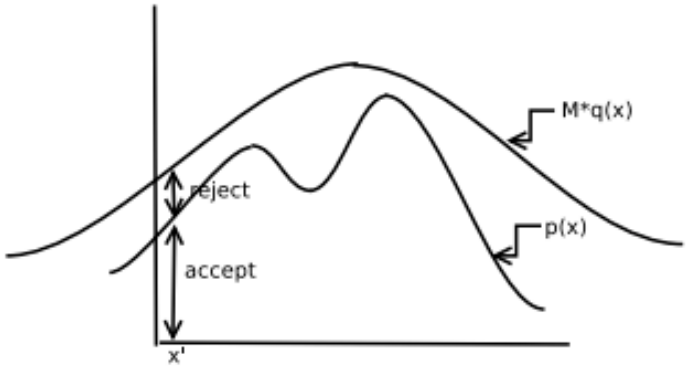


Figure 2-1 Rejection Sampling (Jain 2010)

The distribution q(x) is presumably easier to sample by using the inverse CDF method. We may sample $\xi \cdot M \cdot q(x') \leq p(x')\ then\ x' is\ accepted$ from q(x) as follows: -

$$x' = Q^{-1}\ and\ Q(x) = \int q(x) \tag{2.34}$$

This is then followed by comparing a second random number ξ with the ratio of $\frac{p(x')}{M \cdot q(x')}$ such that if

$$\begin{cases} \xi \cdot M \cdot q(x') \leq p(x')\ then\ x' is\ accepted \\ \xi \cdot M \cdot q(x') \geq p(x')\ then\ x' is\ rejected \end{cases} \tag{2.35}$$

This method ensures that x' is sampled according to the p(x')distribution

2.10.4 Sampling from the exponential distribution using the inverse CDF method

Radioactive decay of a nucleus may be described as an exponential distribution with a decay rate λ given by

$$f(x) = \lambda e^{-\lambda x}$$
$$with\ x \in [0, \infty]\}\ and\ \lambda > 0 \tag{2.36}$$

The CDF is then given by

$$F(x) = \int_0^x \lambda e^{-\lambda x'} dx' = 1 - e^{-\lambda x} \tag{2.37}$$

To sample from an exponential distribution, we take a random sample of u from a uniform distribution on [0,1),

$$u_j = 1 - e^{-\lambda x_j} \tag{2.38}$$

to yield

$$x_j = F^{-1}(u) = -\frac{1}{\lambda} \ln (1 - p_j \tag{2.39}$$

2.11 Law of Large Numbers and Central Limit Theorem

The law of large number expresses the fact that the expectation value of a quantity in a sample distribution converges to the population distribution expectation value for that quantity as the sample size increases. Cashwell and Carter (1975)

Given that the expectation value

$$\langle z \rangle = \int_a^b z(x) f(x) dx \qquad 2.40$$

And the sample mean

$$\bar{z} = \frac{1}{N} \sum_{i=1}^{N} z(x_i) \qquad 2.41$$

then, the law of large numbers indicates that the sample mean approaches the population mean according to

$$\lim_{N \to \infty} \bar{z} = \langle z \rangle \qquad 2.42$$

The variation in the different values of z is given by the sample variance which for large numbers is

$$\sigma^2(z) \cong \frac{1}{N} \sum_{i=1}^{N} [z(x_i) - \langle z \rangle]^2 \qquad 2.43$$

and the standard deviation is the square root of the variance.

The Central Limit Theorem provides an estimate of the uncertainty in the expectation value of a quantity and states that the variation of the sample mean from each simulation is distributed normally about the true population mean for large N. It is represented by

$$\lim_{N \to \infty} Prob \left\{ \frac{|\bar{z} - \langle z \rangle|}{\sigma(z)/\sqrt{N}} \leq \lambda \right\} = \frac{1}{\sqrt{2\pi}} \int_{-\lambda}^{\lambda} e^{-u^2/2} du \qquad 2.44$$

Hence the confidence interval for the true mean E(z) may be specified by

$$\begin{cases} 68\%\ confidence\ interval: & \langle z \rangle - S_{\langle z \rangle} < E(z) < \langle z \rangle + S_{\langle z \rangle} \\ 95\%\ confidence\ interval: & \langle z \rangle - 2S_{\langle z \rangle} < E(z) < \langle z \rangle + 2S_{\langle z \rangle} \end{cases} \qquad 2.45$$

2.12 MCNP Statistics

It is important to distinguish between the precision of estimated quantities obtained from Monte Carlo calculations and its accuracy. The precision is determined by the statistical fluctuations of individual scores around the mean value while the accuracy is a measure of closeness of the value to the true physical quantity of interest.

The accuracy associated with an MCNP calculation is determined by the quality of physical and mathematical models employed in the code, the uncertainty in physical atomic and nuclear data. It is also affected by the actual modelling of geometry, energy and angular distribution. The precision is affected by the number of histories, type of tally and the methods employed in variance reduction. Shultis and Faw (2011). MNCP outputs are often presented with statistics which allows a judgment on the precision of the result. Important statistical quantities in Monte Carlo calculations include: -

2.12.1 Relative error

The relative error is the fractional standard deviation estimated uncertainty in the tally mean and is expressed as

$$R = \frac{S_{\bar{x}}}{\bar{x}} \qquad 2.46$$

R should be < 0.1 for a reliable tally confidence interval. The value of R is determined by two components: - the fraction of history contributing non-zero values to the tally and the dispersion in the non-zero scores. A variance reduction effort aims to increase the scoring efficiency while minimizing the dispersion in the non-zero scores thus minimizing the relative error. It indicates that the uncertainty in the estimate of the expectation value is

proportional to $1/\sqrt{N}$. Hence as the number of histories of an MCNP run is quadrupled, the uncertainty in the estimate of the sample mean is halved.

2.12.2 Figure of merit (FOM)

Another important statistic is the figure of merit given by

$$FOM = \frac{1}{R^2 T} \tag{2.47}$$

where T is the simulation time. Considering that the relative error is inversely proportional to $\sqrt{N}$ and the simulation time is proportional to the number of histories, hence the FOM is independent of N and remains relatively constant except for the early simulation fluctuations. Thus, the FOM is a tally reliability indicator because, for a well-behaved tally, the FOM is constant. For variance reduction options of the same problem, the result with the largest FOM is preferred because the larger the value of FOM, the more efficient the calculation as it takes less time to reach the same value of R.

2.12.3 Variance of variance (VOV)

The VOV is a measure of the accuracy of the relative error and is defined as

$$VOV = \frac{S^2(S^2_{\bar{x}})}{S^2_{\bar{x}}} = \frac{\sum_{i=1}^{N}(z_i - \langle\bar{z}\rangle)^4}{\left[\sum_{i=1}^{N}(z_i - \bar{z})^2\right]^2} - \frac{1}{N} \tag{2.48}$$

As the VOV involves the third and fourth moments of the tally distribution, it is more sensitive to high score values, hence such values must be appropriately sampled to obtain reliable tallies. In MCNP simulations, the VOV is tested for an inverse N dependence and must be less than 0.1 for all kinds of tallies.

2.13 Variance Reduction

The Analog Monte-Carlo approach involves the simulation of each particle and the interactions it undertakes according to the physical laws as it occurs in nature based on the interaction cross-sections. This method is however, not computational efficient and as such calls for optimization in the number of particles to be tracked vis-à-vis the computing time. Variance reduction provides a method for reducing Monte Carlo simulation time by employing an efficient random walk designed to reduce the dispersion of the tally value about the mean with an acceptable relative error. The approach is used to reduce the computational efforts by simplifying the MCNP model through the use of a less detailed geometric model of a region with little influence on the problem being studied. For instance, one can safely discard tracking neutrons that undergo thermalization in case of problem where the fast neutron fluence is sought.

Another approach of non-analog Monte Carlo which involves the modification of the sampling process where the sampling is biased such that events contributing significantly towards the tallying are favored over that which obtains naturally. To ensure that the expectation value remains the same in the non-analog model as in the analog model, the score is modified to remove the effect of biasing by weighting the contribution. The variance reduction techniques employed in the MCNP code may be classified into four categories: -

2.13.1 Truncation methods

This method speeds up simulations by truncating parts of the phase space adjudged not to contribute significantly to the solution of the problem. The truncation method in the MNCP includes the use of CUT command which specifies that photons of energy below are

discarded. The NPS and CTME commands specify that the MNCP code be terminated after a certain number of particle histories have been run or computing time has been exceeded.

2.13.2 Population control methods

An example is the Geometry Splitting with Russian Roulette technique which is a biasing method used to control the number of histories that would potentially produce a non-zero score. This is accomplished by tracking the history through phase space and killing the particle if it enters a sub-region where the likelihood of producing a non-zero score is low. Conversely, in a region of high non-zero score, the history is split to enhance the contribution and reduce the tally variance. In this technique, the importance of a region is indicated in the MCNP model. In Geometry Splitting, when particles move from a less important region to one of greater importance, the number of particles is increased while the weight is halved. For movement to a less important region, particles are killed in an unbiased manner to avoid wasting time. Geometry splitting results in a decrease in history variance but increases time used per history while Russian Roulette generally increases the history variance but reduces the time per history.

2.13.3 Modified sampling methods

In this method, the sampling is altered to increase the number of tallies per particle by the choice of a distribution which sends particles to the desired direction or region of the phase space. Examples of the method include the exponential transform, implicit capture and source biasing.

A common variance reduction technique in radiation transport is the implicit capture which involves launching and tracking packets of particles through different interactions. Each packet is assigned an initial weighting factor of $w_0$before the collision, in implicit capture

the particle always survives the collision with an adjusted particle weight after the collision governed by

$$w_0 \rightarrow \begin{cases} p = \frac{\sigma_s}{\sigma} w' = w_0 \\ p^* = 1 - p \quad w' = 0 \end{cases} \qquad 2.49$$

and

$$\Rightarrow \overline{w'} = pw_0 + p^* \star 0 = \frac{\sigma_s}{\sigma} w_0 \qquad 2.50$$

where p is the probability of the particle being scattered after the collision and σ_s *and* σ represent the scattering and total macroscopic cross-sections respectively. The advantage of the implicit capture technique for variance reduction is that a particle that reaches the tally region is not absorbed just before the tally is made, by using the expected surviving weight, the history variance is reduced. This may adversely affect the FOM as the simulation time is increased because of longer particle history. Saidi *et al* (2013)

2.13.4 Partially deterministic methods

In this method, the normal random walk approach is replaced with deterministic techniques such as next event estimator or by controlling sequence of random number generation. The available method in MNCP includes the Point and Ring Detectors, DXTRANS and correlated sampling.

2.14 Review of Previous Work

Instrumental neutron activation analysis and spectrum parameters study in experimental channels using HEU based research reactors based have been extensively conducted by Jonah *et al,* (2005; 2006). Nyarko *et al*, (2007) reported the development of several analytical techniques based on Ghana MNSR for the determination of heavy metals in

environmental samples and trace elements in geological samples. Owing to nuclear proliferation concerns, a global initiative by the US DOE through the RERTR was formed; with a principal focus to establish a basis for the conversion of research reactors from HEU to LEU without significant changes in reactor operational characteristics and safety margins leading to various works in reactor design and benchmark studies for LEU conversion.

Huda *et al,* (2004) reported on the neutronics analysis of a 3-MW TRIGA MARK II research reactor core and presented a validation of the results obtained by benchmarking with the experimental, operational and available Final Safety Analysis Report (FSAR) values. A full core 3D model of the TRIGA was developed using the MNCP-4C model to convert from HEU to LEU. TRIGA benchmarking experiments were conducted to establish the consistency and accuracy of the Monte Carlo simulation and the underlying neutron transport physics. The utilization of the reactor ranges from basic nuclear research, manpower training to the production of radioisotopes for its uses in agriculture, industry, and medicine.

In a joint feasibility study, Hanan *et al*, (2002) presented a comparison of the results obtained for the core conversion of the HFR-Petten reactor using Monte Carlo analysis and diffusion theory. The results for the shutdown margins and performance indices using the two methods showed good agreement and thus confirmed the adequacy of the approach.

A feasibility study for the conversion of the 10MW, WWR-M research reactor at the Kiev Institute for Nuclear research was carried out by Pond *et al*, (2002) to determine the possibility of converting from HEU (36%) UO2-Al fuel assemblies with (3 tubes, UO_2-Al fuel meat with 1.1 gU/cm^3 and 37.0 g ^{235}U) to candidate LEU (19.75%) fuels consisting of LEU WWR-M2 (3 tubes, UO_2-Al fuel meat with 2.3 gU/cm^3 and 38.3 g ^{235}U) and LEU WWR-MR (37 pins, U9Mo-Al fuel meat with 2.4 gU/cm^3 and 38.1 g ^{235}U) using the

MCNP code. The results obtained for core reactivity, fuel assembly power, experiment flux, fuel-cycle length, the number of fuel assemblies consumed per year, and shutdown margins shows the feasibility of core conversion to LEU.

A computational method based on an MCNP model coupled with the depletion code BURN was reported by Damn and Nabbi, (2002) for the core conversion and fuel element performance analysis of the FRJ-2 research reactor and applied it to a mixed core consisting of HEU and LEU fuels. The result shows consistency with experiment and indicated a lowered thermal flux in the core region of about 19% but flux reduction in the reflector region around the core remained limited to 6%.

A 3D computational model of the Texas A&M University Nuclear Science Center Reactor (NSCR) using the MCNP code and high-temperature cross-section data was developed by Kim *et al*, (2004) A full core modeling with details of the fuel elements and control rod was incorporated and the concept of average fission product was used an approximation of the fission product inventory in the core. The result of the model yielded good agreement with results obtained from an in-house three-dimensional diffusion code and from foil activation measurements.

In a research work by Guotu *et al*, (2009), The MCNP code was used to model the in-hospital neutron irradiator IHNI, an MNSR type reactor designed for boron neutron capture therapy; calculation of the critical mass, control rod worth and reactivity regulators was carried by optimizing materials in the MNCP code. The result of the modelling indicated a satisfactory neutron flux levels at the radiation filters with a thermal flux of 2.14×10^{9} n/cm^{2}s and an epithermal neutron beam 4.0×10^{8} n/cm^{2}s, thus confirming the suitability of the adaptation of IHNI for BNCT. A coupled neutronics analysis and transient code RELAP5

was used to determine the dynamic characteristics of the IHNI for various reactivity insertions.

Aldawahra *et al* (2015) conducted a comparative study of the conversion of the Syrian MNSR from HEU (UAl_4-Al 90% enrichment) to LEU (UO_2-Zr cladding with 12.6% enrichment) using the MCNP4C code with the number of fuel pins kept the same in both cases except for an increase in the control rod material from 0.195 to 0.205 cm. Core calculation of cold core excess reactivity, control rod worth, safety reactivity and thermal neutron flux shows the validation of the LEU as a potential fuel for conversion. In a similar conversion effort for the Iranian MNSR from HEU to LEU using UO_2 enriched to 12.5%, Sichani *et al*, (2006) validated the benchmarked clean cold core with experiments. The predicted result obtained from the MCNP model showed a deviation of 1.6% in the excess reactivity for LEU from the experiments. A further refinement using the validated model indicated that at an enrichment value of 20%, a close agreement between the model output and experiment was achievable by means of changes in the LEU's fuel meat configuration.

As part of the conversion studies on the Ghana MNSR reactor the Monte Carlo transport code MCNP5 was used to optimize a previously developed 3D model of the GHARR-1 reactor Anim-Sampong *et al,* (2006) The result from a neutronics analysis of the 90.2% HEU core was compared with the results for various LEU fuels with enrichment values between 12.6% and 19.75%. The result from the optimized model demonstrates that the model correctly simulates the core neutronics design parameters, hence is effective for performing a global neutronics analysis of the MNSR.

Mahmood *et al,* (2008) reported in their work on neutron analysis for the core conversion of the Pakistan MNSR reactor PARR-2 using transport code WIMS and diffusion code CITATION shows that neutronics analysis yielded a lower flux values at irradiation sites

attributable to spectrum hardening for the LEU fuel, however, from a neutronics viewpoint, an LEU fuel UO2 of 12.6% enrichment with zirconium clad is suitable for converting the HEU while maintaining the same number and dimension of fuel pins.

A comparative neutronics study of PARR-2 HEU core with candidate LEU fuels by Waqar *et al,* (2008) using the same codes WIMS and CITATION indicate good agreement with results obtained from Monte Carlo transport calculations and the axial and radial thermal flux agree with experiments.

In support of the global trend to convert research reactor to LEU, a neutronics analysis of the current HEU core configuration of the Nigerian MNSR NIRR-1 was conducted, the results were validated with the zero-power results and available operational data from the final safety analysis report. A full core model of the NIRR-1 reactor consisting of 347 fuel pins and all reactor components was developed using the Monte Carlo code MCNP-4C Jonah *et al*, (2007). A comparison of the experimental result and the prediction from the MCNP simulation indicates that the developed model is an accurate representation of the reactor core and confirms the suitability of the MCNP model as a basis for conversion studies of qualified nuclear fuels.

A feasibility study to determine the enrichment required for conversion of two LEU UO_2MNSR fuels with enrichment of 12.5% and 12.0% was conducted by Jonah and Ibikunle, (2009). The result showed a close agreement between the 12.5% enrichment and that of the HEU, however, the magnitude of the neutron flux in the inner irradiation channels was between 5% and 12% lower for the two LEU fuels. A reduction in the shutdown margin was observed and a redesign of the control rod was required in this configuration to compensate for the loss of reactivity.

Aside from the MCNP code commonly used in criticality safety calculations, other deterministic codes have been used. Nawaz *et al*, (2012) conducted a comparative neutronics study for a standard HEU and potential LEU and MEU cores using the deterministic code WIMS-D4 and CITATION diffusion codes, the computed core parameters yielded a satisfactory agreement with literature. A core loading of 1110g was required for the HEU core and while 10733.5 g was needed for UO2 with (Zr-clad) and that enrichment values between 19.81% and 24.29% will be required to have the same excess reactivity as the HEU. A similar computational scheme based on the same codes was used by Azande *et al* (2010) to determine the fuel enrichment for NIRR-1. The scheme iterated through various enrichment values for UAl_4 and $UO_2$by varying the core loading of the LEU. Keeping the enrichment less than 20%, and excess reactivity within the design prescription between3.5 and 4.0 mk required an increase in core loading from 946g/cc simulated for the HEU to 1141g/cc for the LEU is required for the UO_2 fuel.

One of the objectives of the conversion program is to design an LEU core with operational capabilities similar to the HEU and ensure that thermal neutron flux in the irradiation channels is not compromised. In a study by Khattab *et al*, (2011), the MCNP code was used to determine the neutronics parameters of the Syrian MNSR, worth of the top beryllium shim, axial neutron flux distribution and the prompt neutron lifetime and the effective delayed neutron fraction. Good agreement was reached between the calculated and the measured result for HEU indicating that the model established is a good representation of the Syrian MNSR. The kinetic parameters are significant in the analysis of the reactor transients. Albarhoum, (2010) investigated the effect of control rod position on the neutron flux in the inner and outer irradiation channels of the Syrian MNSR by means of a

WIMSD/CITATION model and reported a dependence of flux on distance from the control rod axis with no variation with vertical position.

In an analytical study to determine the effect of MNSR core conversion on flux performance and core lifetime with a 12.5% enrichment LEU-UO_2, Liaw and Matos (2006) employed an MCNP model from detailed geometry of the NIRR-1 and reported a decrease of between 7% and 10% in the thermal neutron flux in the inner irradiation channels thus requiring an increase in the operational power level from 30kW to 33kW to achieve the HEU nominal flux level. Fuel depletion rates determined using the diffusion code REBUS in conjunction with top Be shim addition indicate the LEU-UO_2 core can be operated for 23 shim cycles with a cycle length of 2.5 years at 16.5kW power level 23 shim cycles (cycle length of 2.0 years) length for the HEU core.

Change in the reactivity has an important bearing on the operation and safety of a reactor. In a study by (Omar et al, 2012), the feedback reactivity coefficient of the Syrian MNSR was determined using the WIMSD/CITATION code. The WIMSD code was used to calculate the cross-sections of all the reactor components, the group constants were then inserted in the CITATION code to determine the neutron spectrum at different water and fuel temperatures using 69 energy groups. The calculated moderator and fuel temperature coefficients were calculated to be -0.06 x $10^{-3}\Delta k/k/°C$ and -3.2 x $10^{-7}\Delta k/k/°C$ respectively in good agreement with measured values. There was a negligible contribution to the neutron spectrum from the increase in water temperature from 293K to 318K and fuel temperature from 293K to 338K respectively.

As part of safety analyses calculation related to the conversion of the Syrian MSNR from HEU-UAl_4-Al to potential fuels UO_2 (12% and 20%) enrichment respectively, Hainoun *et al,* (2009) employed the difference between two MCNP runs using total neutron and

prompt neutrons only to determine the delayed neutron fraction β_{eff}. The β_{eff} for the HEU core is 0.00732 which differs from the experiment by a factor of 7%. The prompt neutron lifetime obtained using perturbation theory overstates the measured vale of 74.6 x 10^{-6} s by a factor of 25%.

As a follow up study, Nagaya *et al*, (2010) presented a comparison of two Monte Carlo calculation methods proposed by Meulekamp and Nauchi for determining the effective delayed neutron fraction in a reactor and reported that while both methods produce accuracy in results within 2% for thermal systems, the Meulekamp method causes a discrepancy of 5% in fast systems while Nauchi's approach produces good results for fast bare system but a 10% discrepancy for reflected systems.

3 MATERIALS AND METHODS

3.1 Introduction

This chapter contains an overview of the computer code - MCNP5 that were used for this work as well as a general description of the reactor model developed for the study. A detailed description of the MCNP model would be developed to accomplish the primary goal of conversion of the HEU core to LEU by means of the three dispersion fuels: - U_3Si_2, U_3Si, and U9Mo all clad in aluminum.

3.2 Materials

3.2.1 Low-Power Research Reactors

Nation states desirous of developing manpower capabilities in nuclear science and technology often seek to acquire low power research reactor owing to its versatility in a variety of disciplines. These reactors are often employed in applications such as teaching and research, medicine and biology, activation analysis, nondestructive testing, production of radioisotopes.

Low power research reactors LPRR are characterized by power levels of less than 100 kW and neutron flux of the order of 10^{12} n/cm^2.s. A number of factors that engenders the deployment of such reactors include: -

i) Ease of use of such facilities due to the less stringent sample handling requirements

ii) Variety in the sample types ranging from solids, liquids, biological materials, petroleum fluids, wet tissues etc.

iii) Large, non-uniform materials can often be inserted in reactors with a much lower concern of inadvertently introducing high radioactivity induced in the system.

The typical usage of typical low power research reactors may be categorized into the following: -

i) Production of radioisotopes particularly short-lived isotopes, which are useful in tracer research but are often difficult to obtain commercially due to the very short half-lives often less than a few days.

ii) Studies in reactor kinetics and dynamics, nuclear spectrum distribution and responses of detectors to neutrons, gamma and other charged particles can be conducted in reactor characterization.

iii) Research reactors also provide an avenue for the use of extracted neutrons via irradiation channels for dosimetry studies. Neutron beams are used for non-destructive testing of light elements.

A most common utilization of research reactors is the area of Neutron Activation Analysis in which thermal; epithermal or fast neutrons are optimized for the characterization of elements of low concentration.

Other examples are the studies of neutron transport in a media of interest, neutron energy measurement using Cd cutoff gold foils, and multiple foil activation methods, determination of void fraction in multi-phase fluids etc.

Another attraction of research reactors is that they can often be situated more liberally owing to the inherently safe nature of their design by having a large negative temperature coefficient and a small excess reactivity. The acquisition costs of research reactors with a thermal power greater than 1MW exceeds tens of millions of dollars thus putting them beyond financial consideration of many developing countries. Low power research reactors with power $\leq$ 100kW IAEA-TECDOC (1985) costs considerably less while still adequately serving the needs of users in developing countries. Operational, capital and insurance costs

are also much lower. Examples of low power research reactors include Argonaut, Slowpoke, and MNSR.

3.2.2 Description of the MNSR

The MNSR is a small compact, inherently safe low-power nuclear facility embedded in a tank of light water. The fuel element is made of highly enriched uranium with light water serving as both a coolant and moderator. Fuel pins are concentrically located in 10 rings with varying number of dummy rods depending on the specific configuration while four tie-rods on the eighth ring provides structural integrity to the core.

The reactor is composed of five major sections: - the reactor core, the beryllium reflector, the control unit, the auxiliary system and the irradiation facility. The reactor core is of cylindrical geometry embedded in an annular beryllium serving as both a neutron reflector and moderator. The assembly rests on a bottom beryllium block and is cooled by natural convection of water whose inlet is near the interstices between the bottom block and the annular block. The ratio of the height to the radius is about unity to increase the axial neutron leakage at the top thus increasing the worth of the top beryllium shims. The top of the beryllium block is covered with Be shims of varying thickness designed to provide sufficient compensation for the reactivity loss because of burnup and fission fragments poisoning.

Acting as the internal monitoring devices are in-pile detectors such as fission chambers for flux measurements, the thermocouple and platinum resistance thermometer and water level meters.

The most common usage of the reactor is the NAA and this is performed using ten irradiation sites located at a radial distance from the center of the core. The five inner

irradiation sites concentrically located in the Be block can take samples of volume 7cc. The outer irradiation channels are connected with a rabbit sample transfer system for sending samples for irradiation. In view of the low temperature in the sites, samples of biological origin can also be irradiated and analyzed.

The main control of the reactor system is by means of a single centrally located Cadmium absorber rod encased in a steel cladding controlled by means of a pulley and is used for starting and shutting down the reactor, regulating power levels and compensate for fuel burnup. Additional control mechanism is the use of reactivity regulation devices.

3.2.3 Physics Design of the MNSR

The design basis on which the MNSR is premised includes the following: -

a) Low critical mass and compact core size

b) High ratio of neutron flux in the irradiation site to the core thermal power

c) Inherently safety design by means of negative core excess reactivity

The requirement of an inherently safe device necessitates a design based on an under-moderated core of low critical mass which is achieved using highly enriched uranium as fuel material, water as moderator and coolant, beryllium as annular, top and bottom reflectors. The arrangement of the beryllium reflectors helps to reduce the effect of control rod movement on the core reactivity and the flux distribution thereby improving its value for NAA. The need to effectively use the limited excess reactivity while maintaining overall reactor safety necessitates a balance between thermal hydraulics and safety concerns. This leads to the need to reduce the ratio of H to U-235 in the fuel lattice to increase the extent of under moderation of the core thereby increasing the negative moderator temperature effect this enhancing temperature feedback. A complementary

approach is a reduction of the ratio of the core height to diameter to almost unity thereby increasing the axial neutron leakage fraction and thus increasing the worth of the top reflector. It has the value of shortening the temperature feedback time by improving the coupling between the inlet and the outlet flow mixing.

3.2.4 General Description of NIRR-1

NIRR-1 is a tank-in pool Miniature Neutron Source Reactor type reactor designed and installed by the China Institute of Atomic Energy (CIAE). The reactor which went critical on 3rd February 2004 has since been in operation primarily for Neutron Activation Analysis. The reactor core of NIRR-1 consists of 347 fuel elements and arranged in a cylindrical fuel cage. Each fuel pin is a 90.2% enriched uranium-235 alloy extrusion in the form of UAl4 as the fuel meat, with aluminum alloy as clad material. The fuel element is 248 mm in length with the active length being 230mm. The diameter of the fuel meat region is 4.3mm and the loading of U-235 in each fuel rod is 2.88g. The cadmium absorber control rod is 266mm long and 3.9mm width enclosed in a stainless steel clad of thickness 0.5mm. The total length of the control rod assembly is 450mm. Three of the five outer irradiation channels have a diameter of 22mm each while the other has a diameter of 34mm.The fuel cage is enclosed in an annular beryllium reflector placed on a lower beryllium reflector plate. The annular beryllium and the lower reflector are placed to form a lower orifice allowing the convective flow of water through the core.

The reactor vessel is a two-part cylindrical alloy container of 0.6m in diameter and 5.6m height. The vessel is suspended in a stainless steel-lined pool of water made of reinforced concrete. In this study, we shall focus on the feasibility of replacing the HEU core with the following potential LEU fuels: - U3Si, $U3Si_2$, and U9-Mo with Aluminum as clad material.

The details of the NIRR-1 HEU core and characteristics of the fuel pins are presented in Table 3-1.

Table 3-1 Characteristics of the NIRR-1 HEU Core

Core	Fuel pins
347 fuel pins	Fuel meat OD: 4.3 mm
3 dummy aluminum pins	Clad OD: 0.6mm
4 aluminum posts	Clad thickness: 0.6 mm
981 g ^{235}U	Fuel height: 230 mm
90.2% enriched Uranium	^{235}U per pin: 2.88 g
U density in alloy fuel meat	0.94 g/cm3 (~ 27 wt-% U)

Source: FSAR (2005)

3.2.4.1 Flux and Power of the NIRR1

At a maximum neutron flux of 1 x 10^{12} n/cm^2, in the inner irradiation sites, the thermal power is about 31 kW. The clean cold core excess reactivity measured at 20^{o}C is 3.77mK during the commissioning of NIRR1 and the maximum daily operable time was found to be 4½ hours for the cold core.

3.2.4.2 Kinetic Parameters of the MNSR

The kinetic parameters of the MNSR core quoted from the final safety analysis report FSAR (2005) gives the effective delayed neutron fraction $ß_{eff}$ = 8.08 x 10^{-3} while the prompt neutron lifetime = 8.12 x 10^{-5} seconds.

The dimensions of the beryllium reflector and their elemental composition are given in Table 3-2 and Table 3-3 respectively.

Table 3-2 Dimensions of the beryllium reflectors

Dimensions of the beryllium reflectors			
Beryllium reflectors	Outer diameter (mm)	Inner diameter (mm)	Height (mm)
Annular radial reflector	435.0	231.0	238.5
Bottom plate reflector	290.0	25.4	50.0

Source: FSAR (2005)

Table 3-3 Elemental Composition of Beryllium reflector

Material	ppm	Material	ppm	Material	ppm
Be		N	200.0	Li	1.0
BeO	25000.0	Cr	200.0	Dy	1.0
Fe	4000.0	Zn	150.0	Cd	0.5
Pb	3000.0	Ni	100.0	Sm	0.5
Al	3000.0	Mn	20.0	Eu	0.1
Mg	1000.0	Ag	15.0	C	0.1
Si	800.0	Co	10.0		
Cu	200.0	B	2.0		

Source: FSAR (2005)

3.2.5 LEU Dispersion Fuels

Prior to the enrichment initiatives of RERTR, commonly used fuels in research rectors includes UAl_x-Al with uranium densities up to 1.7g/cm^3, U_3O_8-Al with densities of 1.3g/cm^3 and $UZrH_x$ alloy with densities of 0.5g/cm^3. In the case of LEUs, the candidate fuels must have densities much greater than these, owing to the lower enrichment. The existing fuels UAl_x-Al, U_3O_8-Al, and $UZrH_x$ have densities qualified up to 2.3g/cm^3, 3.2g/cm^3 and 3.7g/cm^3 respectively, these values are found to be inadequate in the case of the Pakistan Research Reactor. Newer silicide fuels U_3Si_2-Al and U_3Si are qualified up to 4.8g/cm^3 and 6.0g/cm^3 respectively. (RERTR, 2005) The density value of 4.8g/cm^3 is equivalent to 43-vol% of U_3Si_2 in the fuel meat and is considered a limiting value for commercial production. Other promising options include the U-Mo fuels with densities in the range 6 -8 g/cm^3.

A feasibility study of potential LEU fuels for core conversion of generic MNSR used in research reactors worldwide was carried out by (Matos and Lell, 2005). The choice of fuels considered was based on the fuels' qualification status and the availability of manufacturers capable of producing the fuels. The operational history of power reactors with longer burnup was also taken into consideration.

Preliminary results indicate deviation from the validated HEU core, The deviation necessitated changes in the number of fuel pins, changes in the thickness of the clad and changes in core radius to height ratio. Matos and Lell (2005). In this study, the focus would be on selected dispersion fuels [U_3Si, U_3Si_2, and U_9Mo];

Dispersion nuclear fuels are made of fissionable material dispersed as small particles through a non-fissionable matrix of metal, ceramic or graphite. A schematic diagram of a dispersion fuel is presented in Figure 3-2.

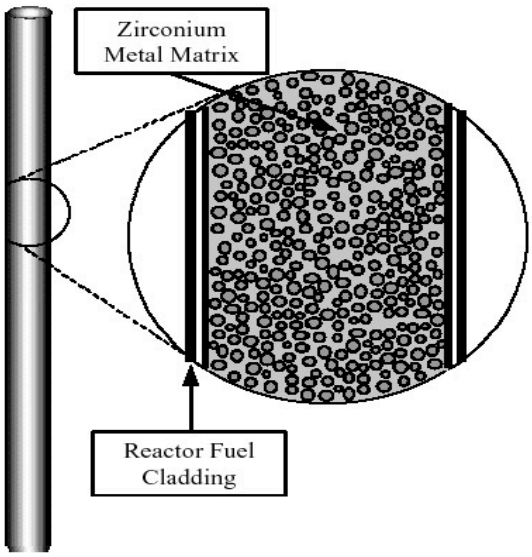


Figure 3-1 Schematic of a Dispersion Fuel

In view of the harsh operating conditions inside a reactor consisting of gas associated with fission, fission fragments, thermal and radiation diffusion, high power densities and the presence of various of radiations, it is important that nuclear fuels material possess high structural integrity, radiation stability and good thermal conductivity without adversely affecting its fission rates. Dispersion fuels are characterized by high power densities and near maximum fission densities at near end of life. The following are the benefits accruing from the use of dispersion nuclear fuels as against the commonly available commercial fuels: -

i) Improved Structural Integrity

In a typical nuclear fuel used in many LWR such as UO_2 with zircaloy cladding, the ceramic solid oxide fuel pellets are of low thermal conductivity and as such are subjected to very high temperature variation in the reactor core leading to structural changes in the fuel that cause migration of atoms and gas bubbles.

A dispersion fuel, however, possesses a structural advantage over the solid oxide fuel owing to the widespread distribution of fuel particles in the metal matrix. The high thermal conductivity of the matrix implies a more efficient heat transfer within the fuel leading to overall lower operating temperatures and sturdier structural integrity.

Owing to the relative abundance of the matrix in the fuel-matrix admixture, damage due to the production of fission fragment is confined to the tiny microspheres distributed in the matrix and as such limited within the range of fragments.

Dispersion fuels are made up of fuel materials broken up into small pieces' size < 100 um and interspersed in non-reactive matrix materials forming a two-phase mixture of fuel and the matrix, damage due to fission events can, therefore, be contained in the fuel material without affecting the matrix thus increasing the stability.

ii) Containment

The dispersion process guarantees that the fission fragments and gases produced owing to irradiation are contained in the microspheres in the matrix thereby obviating the need for additional gap or voids between the fuel and the cladding. Owing to the localization of the fission fragments, there exists a large portion of the matrix that is completely linked and undamaged thereby providing the fuel with the structural stability, integrity, resistance to corrosion and strength. Holden (1967)

iii) Design Flexibility

The use of the dispersion fuels has an additional benefit in allowing for flexibility in the choice of a matrix material. Hence, matrix materials may be selected to reflect the reactors operating conditions.

The flexibility in the choice of the matrix materials affords the designer the greater opportunity in the selection of both matrix and fissionable material to suit the needs of the reactor. A typical choice of a matrix is aluminum owing to its abundance and high thermal conductivity properties.

iv) Disposal of Weapon-Grade Fuel

In addressing the concern on nuclear non-proliferation and the destruction of waste plutonium fuels, a method employed in fuel production is the dispersion of small microspheres embedded in an inert matrix which is then burned in a nuclear reactor for the generation of electricity

3.2.5.1 Challenges from the Use of Dispersion Fuels

The complex nature of the dispersion fuel, however, implies a comparatively more difficult and expensive fabrication process as against a homogenous UO_2 fuel pellet. This, in the long run affects the recycling of the fuel since it is would be required that the non-fissionable matrix be dissolved in order to have access to the fuel particles. The common practice is, therefore, to burn the fissionable content in the fuel to as low a value as possible prior to disposal.

A summary of the potential fuels is given in Table 3-4. Prior to this study, the only feasibility studies for core conversion of NIRR1 have been based on the use of UO_2. This work, however, focuses on the core conversion of NIRR1 using U_3Si_2-Al, U_3Si-Al, and U9Mo-Al dispersion LEU fuels.

Table 3-4 Potential LEU fuels for Research Reactors

	Fuel type	Density of dispersed phase	Wt.-% U in dispersed phase	U density in dispersed phase	Max. LEU density in fuel meat (g U/cm^3)
1	U-Al alloy fuel	5.7	64	3.7	1.0
2	UAl_x-Al dispersion fuel	6.4	70	4.5	1.7
3	U_3O_8-Al dispersion fuel	8.2	85	7.0	2.6
4	UO_2-Al dispersion fuel	~ 9.5	88	8.4	3.2
5	U_3Si_2-Al dispersion fuel	12.2	92.5	11.3	4.3
6	U_3Si-Al dispersion fuel	15.2	96	14.6	5.5
7	U9Mo-Al dispersion fuel	17.3	91	15.7	6.0
8	UO_2 pellets in Zircaloy clad	10.6	88	9.3	9.3
9	U9Mo monolithic wires clad in Al	17.3	91	15.7	15.7

Source: Matos and Lell (2005)

3.2.5.2 U_3Si-Al and U_3Si_2-Al Dispersion Fuels

Silicide fuels are commonly used in most research and test reactors owing to its uranium density and ease of production and fabrication. U_3Si_2 has been successfully fabricated by Babcock and Wilcox in the US, CERCA in France and Nukem in Germany amongst others.

Safety evaluation report indicates that U_3Si_2-Al is highly qualified for use in non-power reactors and currently being used in many research reactors worldwide. NUREG-1313, (1988). Test conducted with low-enriched U3Si2-Al dispersion fuels at Oak Ridge National Laboratory indicate that the fuel would perform competently in comparison with UAl_x-Al and U_3O_8 high-enriched fuels at operating power densities in ORR. Copeland *et al*, (1987)

HEU based MNSR reactors use extruded pins containing U-Al alloy fuel meat with a uranium density of ~ 0.94 g/cm^3 and a uranium enrichment of ~ 90%. In order to maintain the same dimension and the number of fuel pins as the current HEU, optimization calculations for the uranium density needs to be carried out to determine the value required to match the excess reactivity.

The uranium silicide compounds of interests are U_3Si_2 with a density of 11.3g/cm^3 and U_3Si with a density of 14.91g/cm^3 with relatively high melting points of 1665^{0}C and 930^{0}C respectively. U_3Si_2 has been demonstrated to be more stable under irradiation than U_3Si. Aluminum dispersion fuels have comparatively higher uranium loading than UAl_x-Al dispersion fuels.

It is known that Uranium silicide dispersion fuels undergo excessive swelling at a temperature of 500^{0}C or greater in power reactors, while rapid swelling occurs at fuel temperatures in the region of 900^{0}C which may take place under a loss of coolant accident. Ippolito, (1990) However, the operating temperature in the MNSR is not expected to be close to this.

3.2.5.3 U9Mo-Al Dispersion Fuel

The search for potential fuels with higher density suitable for conversion to LEU led to the consideration of U9Mo dispersion fuels (with density in the range of 6-8 g/cm^3) thus promising a near unlimited LEU burnup. Matos and Lell (2005) indicate that U concentration in U-Mo can reproduce the core lifetime of the original HEU.

This fuel also demonstrated an excellent behavior under irradiation compared to the silicide dispersion fuel; it maintains a stable swelling at temperatures up to 300^{0}C. Irradiation tests

conducted at Idaho National Laboratory's Advanced Test Reactor (ATR) to investigate the performance of candidate fuel materials shows that (U-Mo) with between 6 and 12 wt% molybdenum constitutes the ideal base for further fuel development activities. This study considers the use of U-9Mo/Al as a candidate dispersion fuel for conversion.

There exists however radiation-induced microstructural change that occurs as a result of diffusion between U-Mo Alloy and the Al interaction layer, thus effectively lowering the thermal conductivity of the fuel meat. The use of larger U-Mo particle dispersed in Al is shown to mitigate the thermal degradation effect associated with the interaction layer growth. Ryu et al (2008).

3.3 Methodology

3.3.1 The Monte Carlo Transport Code

In this study, neutronics calculations will be performed using MCNP5, a general particle transport code developed and maintained by the Applied Physics Division at Los Alamos National Laboratory and distributed through the Radiation Safety Information Computational Center (RSICC) in Oak Ridge, Tennessee (Briesmeister, 2000).

The MCNP code has the desirable feature of modeling complex geometry in three dimensions. The neutron energy regime covered in the code range from 10^{-11}-20 MeV for all isotopes and up to 150 MeV for some isotopes Jonah *et al*, (2007). The photon energy regime is from 1 keV to 1 GeV. The Monte Carlo method is formulated as a stochastic model of physical phenomena, without requiring the rigorous derivation of the transport equation. Brown *et al,* (1984). It is suitable for complex geometries and is capable of treating 3-dimensional geometry in a reasonable computing time frame. Briemester, (1993).

A starting point for the Monte Carlo is the integral form of the linear time-independent Boltzmann transport equation 2.16in the form,

$$\Psi\left(\vec{r},\vec{E}\right) = \int\left[\int \Psi\left(\vec{r}',\vec{E}'\right).C\left(\vec{E}'\rightarrow\vec{E},\vec{r}\right)d\vec{E}' + Q(r,E)\right]\cdot T\left(\vec{r}'\rightarrow\vec{r},\vec{E}'\right)d\vec{r}' \qquad 3.1$$

3.3.1.1 The MCNP Input File

The input to the MCNP consists of several files with the main one being the INP file containing the basic information such as geometries, material composition, and tally information required to describe the problem under consideration. Each line or card of the input consists of up to 80 characters. The INP files are of two types: - the first used to set-up an MCNP calculation and referred to as the INITIATE-RUN while CONTINUE-RUN is used to continue running neutron histories in a previously terminated problem. The format of the MCNP input file consists of three sections: the cell card section, the surface card section and the data card section. A full description of the MCNP input and syntax is contained in the MNCP manuals. X-5 Monte Carlo Team, (2005).

3.3.1.2 Cell Card Section

The cell card section defines all cells which are volumes of space obtained by combining logically the 'surfaces' provided in the surface card section. The composition and density of the materials in the cell are identified by the material number. The format for the cell is given below.

The format for the cell card used in the input is given by:

$$j \qquad m \qquad d \qquad geom \qquad Params$$

where

j = cell number starting from $1-5$ column

m = material number which is denoted by 0 for a void cell.

d = is the density of the cell material

1. blank for a void cell
2. positive entry for density in form of atom density in (atoms/b-cm)
3. negative entry for mass density in (g/cc)

$geom$ = list of all signed surface numbers and Boolean operators that specify the cell.

$Params$ = optional specification of the cell parameters.

3.3.1.3 Surface Card Section

The surface cards are denoted in the format below

$$j \qquad a \qquad list$$

where

j = Surface number (column 1-5)

a = surface mnemonic (plane, sphere, cylinder, etc.)

$list$ = numbers that describe the surface (dimensions, radius, etc. in cm). The surface definition for different geometries given in the MCNP code and employed in our model of the MNSR is presented in Table 3-5 below.

Table 3-5 MCNP Surface Cards

Mnemonic	Type	Description	Equation	Card Entries
P	plane	general	$Ax + By + Cz - D = 0$	ABCD
PX		normal to x-axis	$x - D = 0$	D
PY		normal to y-axis	$y - D = 0$	D
PZ		normal to z-axis	$z - D = 0$	D
SO	sphere	centered at origin	$x^2 + y^2 + z^2 - R^2 = 0$	R
S		general	$(x - \bar{x})^2 + (y - \bar{y})^2 + (z - \bar{z})^2 - R^2 = 0$	$\bar{x}\bar{y}\bar{z}$ R
SX		centered on x-axis	$(x - \bar{x})^2 + y^2 + z^2 - R^2 = 0$	$\bar{x}$ R
SY		centered on y-axis	$x^2 + (y - \bar{y})^2 + z^2 - R^2 = 0$	$\bar{y}$ R
SZ		centered on z-axis	$x^2 + y^2 + (z - \bar{z})^2 - R^2 = 0$	$\bar{z}$ R
C/X	cylinder	parallel to x-axis	$(y - \bar{y})^2 + (z - \bar{z})^2 - R^2 = 0$	$\bar{y}\bar{z}$ R
C/Y		parallel to y-axis	$(x - \bar{x})^2 + (z - \bar{z})^2 - R^2 = 0$	$\bar{x}\bar{z}$ R
C/Z		parallel to z-axis	$(x - \bar{x})^2 + (y - \bar{y})^2 - R^2 = 0$	$\bar{x}\bar{y}$ R
CX		x-axis	$y^2 + z^2 - R^2 = 0$	R
CY		y-axis	$x^2 + z^2 - R^2 = 0$	R
CZ		z-axis	$x^2 + y^2 - R^2 = 0$	R

Source: Shultis et al 2011

3.3.1.4 Data Card Section

The data section contains different types of card definitions. The material card provides the specification of the materials filling the various cell regions identified in the CELL cards and is denoted by a unique material number, an elemental or isotopic composition of the materials and the cross-section representative of the material. The nature of the particles to be tracked is given via the MODE card. The specific calculation and the quantities of interest sought required by the user is specified by different tallies cards. As the MCNP code is used for different types of computations, in this work, the interest is criticality calculation which is denoted by the KCODE card. Other commonly used cards in this

section include the source specification cards such as SDEF and KSRC, the importance card and cards describing problem cut-off.

A typical format of the material card is given by

$$Mm \quad ZAID_1 fraction_1, \qquad ZAID_2 fraction_2, \ldots\ldots\ldots$$

where

Mm = material card name (M) followed immediately by the material (m) on the cell card.

$ZAID$ = atomic number followed by the atomic mass of the isotope

$fraction$ = nuclide fraction (positive for atom fraction, negative for weight fraction).

3.3.1.5 Criticality Calculation using the MCNP Input File

The MCNP input being a criticality problem is run using a KCODE card describing the number of particle history and the number of cycles involved. The initial guess of the eigenvalue and the number of inactive cycles to be skipped to ensure convergence is reached is also presented. The format is

$$KCODE \quad NSRCK \; RKK \; IKZ \; KCT$$

where:

$NSRCK$ = the number of source histories per cycle

RKK = the initial guess for k_{eff}

IKZ = the number of cycles to be skipped before beginning tally accumulation

KCT = the number of cycles to be done.

In this work, the run was for 500,000 particles over 430 cycles with an initial guess for k_{eff} as 1.004 and 30 cycles skipped represented in the input file as:

KCODE 500000 1.004 30 430

3.3.1.6 Tallies in MCNP

Tallies are used to extract useful information while tracking particles inside a system. This is done by scoring and cumulating events such as collisions, absorption and dividing the cumulated score by the total number of particles run.

As part of its numerous output options, the MCNP codes provides standard tally types for different problems set as shown in Table 3.1. These tallies are generally used in MCNP calculations to provide detailed information of the parameters of interest and which is dependent on the nature of the problem. The tally results are generated through the collection of relevant data along individual particle such as flux averaged over a cell, current across a surface, flux at a point, energy deposition averaged over a cell, etc. X-5 Monte Carlo Team, (2003) In this study, the tally of interest is the track length estimate of cell flux, F4.

The track length estimate of the neutron flux in a cell as given in F4 is

$$F4 = \frac{1}{V}\int_V dV \int_E dE \int_{4\pi} d\Omega\, \Phi(\vec{r}, E, \Omega) = \frac{WT_l}{V} \qquad 3.2$$

in units of particles/cm^2, where W is the particle weight and the T_l is the track length in cm. The quantity *F4 changes the units into an energy tally and is given below in equation

$$*F4 = \frac{1}{V}\int_V dV \int_E dE \int_{4\pi} d\Omega\, \Phi(\vec{r}, E, \Omega) = \frac{WT_l E}{V} \qquad 3.3$$

The power distribution in the fuel region can be obtained using the tally F4:N which gives the track length estimate of fission heating in a cell or fission energy deposition in a cell. To differentiate between tallies, a comment card is introduced in the form of FC. An FC4 card is merely a descriptive comment card and has no effect whatsoever on the calculation. The

comment entered after FC4 will appear as the title heading of the F4 tally. While an F4:N card specifies that the neutron flux over cell is desired, FS4 is used for sub-dividing a segment for tally purposes. The SD4 card known as the segment divisor is used to further specify volumes and areas for specific tallies. The E4 card is the energy card required to specify energy bins of interest. Tallies of the same kind are uniquely identified by specifying the F$ cards in increment of 10. Hence similar neutron flux tallies may be indicated by: $F4:N, F14:N, F34:N, F54:N$.

In this work, tallies were constructed for neutron flux using a three-group energy structure; 0 – 0.625eV (thermal neutrons), 0.625eV – 0.825MeV (epithermal neutrons) and 0.825MeV – 20MeV (fast neutrons) and normalized and this is represented in the input file as

E4 6.25E-7 8.25E-1 20.0

A summary of the available tallies in the MCNP5 code is given in Table 3-6 below. The MCNP code also generates standard summary information for each simulation and gives the user a better insight of the physics of the problem and the adequacy or otherwise of a proposed model. X-5 Monte Carlo Team, (2003).

Table 3-6 Types of Tallies available in MCNP

Mnemonic	Tally Type	Particles pl	Fn Units	*Fn Units
F1:pl	surface current	N or P or N, P or E	#	MeV
F2:pl	average surface flux	N or P or N,P or E	$\#/cm^2$	MeV/cm^2
F4:pl	average flux in a cell	N or P or N,P or E	$\#/cm^2$	MeV/cm^2
FMESH4:pl	track-length tally over 3d mesh	N or P or E	$\#/cm^2$	MeV/cm^2
F5a:pl	flux at a point or ring	N or P	$\#/cm^2$	MeV/cm^2
FIP5:pl	pin-hole flux image	N or P	$\#/cm^2$	MeV/cm^2
FIR5:pl	planar radiograph flux image	N or P	$\#/cm^2$	MeV/cm^2
FIC5:pl	cylindrical radiograph flux image	N or P	$\#/cm^2$	MeV/cm^2
F6:pl	energy deposition	N or P or N, P	MeV/g	$jerks/g$
F7:pl	fission energy deposition in a cell	N	MeV/g	$jerks/g$
F8:pl	pulse height distribution in a cell	P or E or P, E	pulses	MeV

Source: Shultis et al 2011

3.3.2 Monte Carlo Simulation

The sustenance of a chain reaction in a critical system is characterized by k_{eff} which is the eigenvalue to the neutron transport equation given in Eq. 2.22. The Monte Carlo eigenvalue calculations begin with a system containing a batch of neutrons in a fissionable material, the batch is tracked through many neutron generations. In each batch, a random walk treatment of the particle history is carried out from birth through fission to death through capture or leakage. A probability distribution function describing the physical interactions is sampled to identify the various stages of fission, scattering or capture in the random walk simulation. In a criticality calculation, the initial distribution is obtained from one of the source definition methods of SDEF, KSRC or SRCTP file, for subsequent cycles, the

source points are taken as the points that are written down at collision sites resulting from neutron transport which then serves as the neutron source to the next generation of neutrons produced by fission. Unlike in the MCNP fixed source problems where the source distribution is static, in the case of criticality calculation, the sources changes every cycle.

At each collision point, the following calculation is carried out: - three prompt neutron lifetimes are cumulated, where fission occurs, the three k_{eff} estimates (collision, absorption, and track-length) are computed and the fission sites at each collision is stored for use as source points in the next cycle. The fission energy of the next cycle neutron is sampled separately for each source point and recorded for the next cycle. In addition, the collision nuclide and reaction are also sampled, since fission is treated as a capture reaction, it is not allowed to occur and thus not included in the sampling. From the initial guess of the fission source spatial distribution indicated by the KCODE card, the neutron histories is followed to produce the next batch of fission neutrons and the process is continued until convergence of the fission source distribution to a stationary state, after which the commencement of tallies of interest such as k_{eff} and reaction rates is carried out. The process is then continued until the desired level of uncertainty is reached.

The estimated eigenvalue from Eq. 2.24 may then be written as

$$k^{n+1} = k_0^n \left[1 - b\left(\frac{k_1}{k_0}\right)^n \left(1 - \frac{k_1}{k_0}\right) + \cdots\right] \qquad 3.4$$

Where k_0 is the fundamental eigenvalue of the exact transport solution and k_1 is the eigenvalue for the first higher mode and b is a constant. The definition of k_{eff} in MCNP being the ratio of the number of fission neutron in a generation to the number of fission neutrons in a previous generation is given by

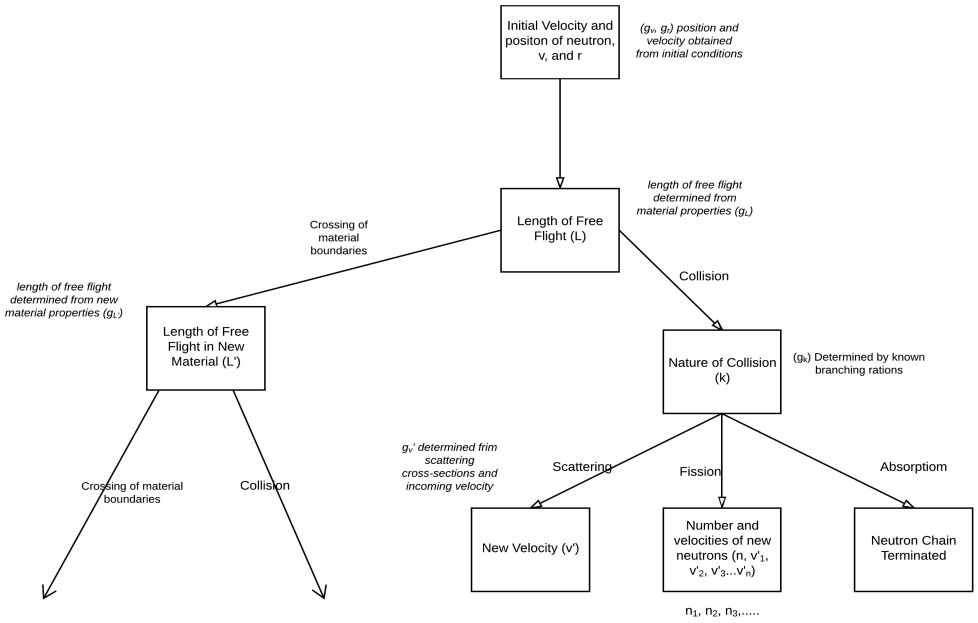
$$k_{eff} = \frac{\rho_a \int_V \int_0^\infty \int_E \int_\Omega v\sigma_f \Phi dV dt dE d\Omega}{\int_V \int_0^\infty \int_E \nabla \cdot J dV dt dE d\Omega + \rho_a \int_V \int_0^\infty \int_E \int_\Omega (\sigma_c + \sigma_{f+} \sigma_m) \Phi dV dt dE d\Omega} \quad 3.5$$

X-5 Monte Carlo Team, (2003), where the phase-space variables are t, E, and Ω for time, energy and direction and position is implicitly represented by r in the incremental volume dV. The denominator is the loss term which is the sum of the following terms: - from leakage, capture, fission and multiplicity (n,xn) terms. The prompt removal lifetime in MCNP is defined as

$$\tau_r = \frac{\int_V \int_0^\infty \int_E \int_\Omega \eta \Phi dV dt dE d\Omega}{\int_V \int_0^\infty \int_E \nabla \cdot J dV dt dE d\Omega + \rho_a \int_V \int_0^\infty \int_E \int_\Omega (\sigma_c + \sigma_{f+} \sigma_m) \Phi dV dt dE d\Omega} \quad 3.6$$

Where η is the population per unit volume per unit energy per unit solid angle.

The decision points in the MCNP simulation is given the Figure 3.3 below



Source: Metropolis and Ulam, (1949)

Figure 3-2 Monte Carlo Decision Points

The following best practices by Brown (2009), have been suggested for adoption in MCNP criticality calculations, all of these suggestions are employed in this study: -

i) The guess of the initial sources is made such that there is a uniform distribution in all fissionable regions to avoid the need for more cycles needed to assure convergence

ii) For applications involving only k_{eff}, it is necessary to determine the proper number of cycles to discard before commencing the tallying of k_{eff}

iii) For applications where both k_{eff} and local tallies are required (i.e. local reaction rates, fission distribution, foil measurements and dose fields), an examination of both the plots of k_{eff} vs cycle and H_{src} vs cycles is needed to determine the required number of cycles that must be discarded before commencing tallying as the use of few discarded cycles would lead to result bias where H_{src} is the Shannon entropy of the fission source distribution.

3.3.3 Monte Carlo Estimates

The eigenvalue k_{eff} and the prompt neutron lifetimes obtained using the MNCP is determined from three correlated estimators: - collision, absorption and track-length estimators, the combination of which gives the best means of calculating k_{eff} and its confidence intervals. X-5 Monte Carlo Team, (2005)

The collision estimator for an active cycle is given by

$$k_{eff}^{C} = \frac{1}{N}\sum_{i} W_i \left[\frac{\sum_k f_k \bar{v}_k \sigma_{fk}}{\sum_k f_k \sigma_{Tk}}\right] \qquad 3.7$$

where i is summed over all collisions in a cycle where fission is possible

k is summed over all nuclides of the materials involved in the i^{th} collision

σ_{Tk} = total microscopic cross-section

σ_{fk} = microscopic fission cross-section

$\overline{v}_k$ = average number of prompt or total neutrons produced per fission by the collision nuclide at the incident energy

f_k = atomic fraction for nuclide k

N = nominal source size for cycle

W_i = weight of particle entering a collision

The absorption estimator, however, is determined when there is an interaction between a fissionable nuclide and a neutron, this estimator differs between cases of analog absorption and implicit absorption and is expressed by: -

$$k_{eff}^{A} = \begin{cases} \frac{1}{N}\sum_{i} W_i \overline{v}_k \frac{\sigma_{fk}}{\sigma_{Ck} + \sigma_{fk}} (for\ analog\ absorption) \\ \frac{1}{N}\sum_{i} W'_i \overline{v}_k \frac{\sigma_{fk}}{\sigma_{Ck} + \sigma_{fk}} (for\ implicit\ absorption) \end{cases} \quad 3.8$$

where i is summed over each analog absorption event in the kth nuclide/or over all the collisions in which fission is possible

$W'_i = W_i \frac{\sigma_{Ck} + \sigma_{fk}}{\sigma_{Tk}}$

While the collision estimator is based on the expected value at each collision, the absorption estimator, however, depends on the events that are sampled at a collision site, hence all collisions contribute to k_{eff}^{C} as against k_{eff}^{A} in which contributions occurs only for an actual fission event for a sampled event in the case of analog absorption.

The track-length estimator k_{eff}^{TL} is tallied whenever a neutron traverses a distance d in a fissionable material and is given by

$$k_{eff}^{TL} = \frac{1}{N}\sum_{i} W_i \rho d \sum_{k} f_k \overline{v}_k \sigma_{f_k} \quad 3.9$$

where i is summed over neutron trajectories

ρ is the atomic density in the cell

d is the trajectory track from the last event

3.3.4 NIRR1 MCNP Model

An MCNP-4C model for the NIRR-1 was developed Jonah *et al*, (2007) based on engineering data from the Final Safety Analysis Report. FSAR (2005) The model was flexible enough to accommodate future modifications. In the model, the center of the reactor core is located at the origin (0,0,0) in the xyz Cartesian coordinates system where the fuel elements are located parallel to the z-axis. Cells were defined for each reactor component such as the fuel elements, the aluminum dummies, the tie rods, control rods, light water as the moderator and pool water, the grid plates, the beryllium reflectors, shim trays, the inner and outer irradiation channels, reactivity regulators and fission chambers. Details of the aluminum support structure, reactor vessels, reactor pool and pool water and the stainless-steel liner were modeled according to the FSAR (2005).

A horizontal and vertical cross-section of the MNSR are presented in Figure 3-3 and Figure 3-4

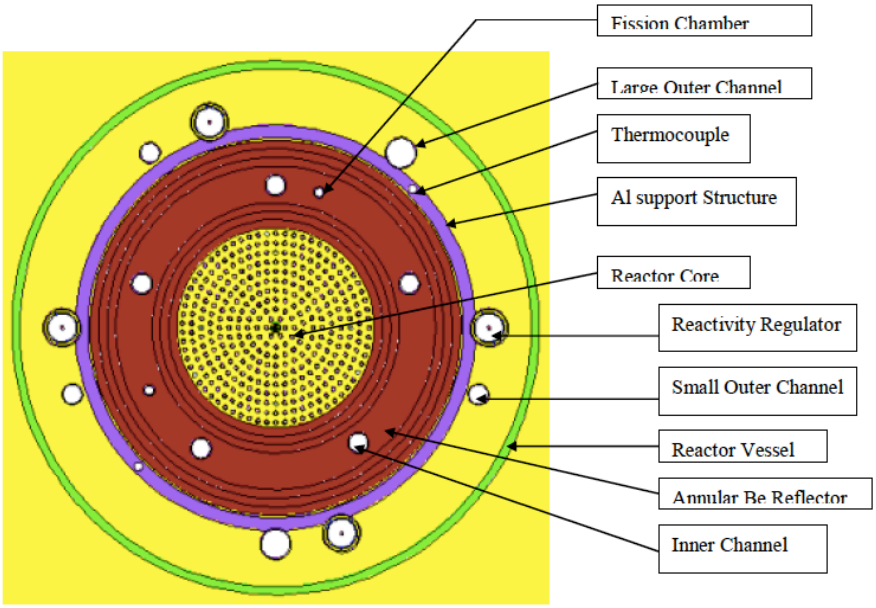


Figure 3-3 Cross Section of the MNSR Core - Source FSAR(2005)

The model was also used for feasibility conversion studies using UO_2 pellets enriched to about 12.5% Jonah *et al*, (2009). In this work, the core of NIRR-1 will be remodeled using recent cross section data available in the MCNP5 version 1.6 through optimizing calculations of the three different dispersion fuel options.

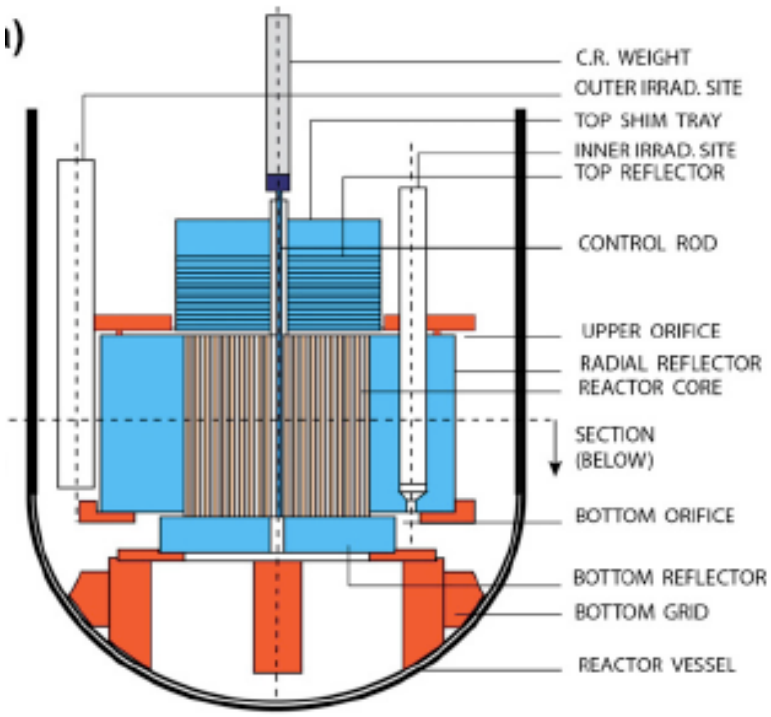


Figure 3-4 MNSR Vertical cross - Source FSAR (2005)

The continuous cross-section data from ENDF/B-VI will be used to model the NIRR-1 core. All calculations will be made using the full energy spectrum available in the MCNP5 code library at 27°C, normal pool temperature. The continuous neutron energy interaction data from ENDF/B-VI cross-section library for 300 K will be used and where not available the data from ENDF/B-V is used.

$S(\alpha,\beta)$ treatment for light water at 300 K will be employed.

The MCNP code is employed to construct a full core 3D model of NIRR-1 LEU consisting of the fuel rods positioned accurately, dummy fuel rods, reactor vessel, tie rods, top and lower grid plates, annular beryllium reflector, bottom beryllium reflector and ten irradiation sites. All fuel elements and irradiation sites were represented as cylinders using the appropriate material composition and dimensions, positioned at exact locations. The

power level of NIRR-1 is controlled by means of the cadmium central control rod which was explicitly modeled along the active length of the rod, the control rod guide tube was also included in the model. The thickness of the water pool employed in the model was considered up to the concrete wall. In the modeling, the center of the core was taken as the origin in the x and y plane and the center of the fuel in z plane. Three different cards were defined comprising of cell card, surface card, and material card. Cells were created for the various components of the reactor bounded by surfaces. Each cell is filled with a material. In other to determine axial neutron flux distributions in the fuel pins, fission chambers, and irradiation channels, relevant tallies cards F4 were constructed.

3.3.5 Kinetic Parameters of the MNSR

Safety consideration in the operation of a research reactor demands the calculation of kinetic parameters such as prompt neutron lifetime and effective delayed neutron fraction. We employed the following features of the MCNP to determine the kinetic parameters of interest:

3.3.5.1 Prompt Neutron Lifetime

The **1/v absorber insertion method** developed at ANL reported by Bretscher, (1997) was used to determine the prompt neutron lifetime through the introduction of a small, dilute and uniform distribution of a pure 1/v absorber into all the materials of the reactor, the negative change in reactivity due to the absorber is then determined by calculating the change in k_{eff} using the equation

$$l_p = \lim_{N \to 0} \frac{\delta k}{k_p} / \left(N \sigma_{ao} v_o \right) \qquad 3.10$$

where

$$\frac{\delta k}{k_p} = k_0 \int_v \left[\sum_j \phi_j \phi_j^* \delta \sum_a \right] dv / PD = N \sigma_{ao} v_o k_o \int_v \left[\sum_j \phi_j \phi_j^* / v_j \right] dV / PD \qquad 3.11$$

and N is the concentration of the absorber in (atoms/b.cm), σ_{ao} is the absorption cross-section at speed v_o and k is the effective multiplication factor. Jonah *et al* (2007) reported perturbation of the reactor with δk determined from k_{eff} at ^{10}B at $4x10^{-8}$ and $6\ x10^{-8}$atoms/b.cm respectively.

The **adjoint method** derives from the reactor point kinetic equation and employs an enhanced feature of the MNCP in version 5-1.60 Kiedrowski *et al*, (2010) through the kinetics option KOPTS card by calculating the tallies integrals over space, energy, and angles and weighted by the flux and adjoint flux. Hanson and Diamond (2012)

$$l_p = \Lambda . k_{eff} = \frac{\langle \varphi^*, {}^1/_v \varphi \rangle}{\langle \varphi^*, F\varphi \rangle} . k_{eff} \qquad 3.12$$

Where φ is the forward flux, $\varphi^*$is the adjoint flux, Λ is the neutron generation time and F is the total fission operator. The KOPTS is placed between KCODE and PRDMP cards in the MCNP deck, the syntax is

KOPTS BLOCKSIZE = 10 KINETICS = YES PRECURSOR = YES.

In ***neutron pulse method***, the MCNP code is used to calculate the prompt neutron lifetime l_p by determining the decay of a pulse of neutrons in a subcritical nuclear reactor assembly through a solution of the equation below: -

$$N = N_0 e^{\frac{(\rho-\beta)}{l_p} t} \qquad 3.13$$

Where N_o is the initial neutron population at time zero for the fundamental node and t is the decay time, ρ is reactivity while β is the delayed neutron fraction. Hanson and Diamond (2012)

3.3.5.2 Effective delayed neutron fraction

In a typical KCODE criticality calculation, the default value for TOTNU card in MCNP deck is YES implying that the total number of neutrons is used. The value of effective delayed neutron fraction β_{eff} may be determined from

$$\beta_{eff} = \frac{k_{yes} - k_{no}}{k_{yes} k_{no}} \qquad 3.14$$

where k_{yes} and k_{no} represent the effective multiplication factors with TOTNU card turned on and off respectively. The use of the KOPTS card also gives an indication of the value of β_{eff}.

In this work, compared the 1/v absorber insertion method and the adjoint flux weighting methods and the TOTNU NO card, the result of which is benchmarked with experiment and then extended for the LEU fuel options.

3.3.6 Parallel Processing in Monte Carlo

Monte Carlo transport simulations are historically time-consuming and highly dependent on the availability of powerful computing resources. With the advent of affordable personal computing devices, such calculations are now easily accessible to research facilities all over the world, this is made possible in view of the inherently parallel nature of Monte Carlo method where particles are independently simulated and calculations speedup is a linear function of the number of processors.

The common approaches for MCNP parallel calculation are the distributed parallelism (message passing) of Parallel Virtual Machines (PVM), which originated from Oak Ridge National Laboratory and the Message Passing Interface (MPI) developed by a collaboration of institutions under the MPI Forum. While each parallel processing method has its strong points, the choice of which to deploy was in our environment dependent on the available

computing resources. A comparison between the MPI and PVM approaches is given in Table 3-7 below.

Table 3-7 Comparison of PVM and MPI parallel processing methods

PVM	MPI
Virtual machine concept	No such abstraction
Simple message passing	Rich message support
Communication topology unspecified	Support logical communication topologies
Inter-operate across host architecture boundaries	Some realizations do not interoperate across architectural boundaries
Portability over performance	Performance over flexibility
Resource and process control	Primarily concerned with messaging
Robust fault tolerance	More susceptible to faults

With the need to achieve the benefits of parallel processing, every line of the MCNP5 code was rewritten with compliance to ANSI standard FORTRAN 90 with dynamic memory allocation capabilities and with strict adherence to the MPI message passing interface mechanism using the OpenMP standard for threading (for shared-memory parallelism). Thus, the MCNPv5 can execute sequentially (no parallelism) or in parallel using only MPI message-passing, using only OpenMP threads, or using both MPI and OpenMP. Brown *et al*, (2002).

Both parallel processing approaches consist of a Master node and Slave nodes. The Master node is responsible for the initialization of the problem, spawning of the sub-tasks and collection and presentation of the output, while the slave node is responsible for actual execution of the assigned tasks. For improved efficiency in the calculation, an MCNP

problem run in either PVM or MPI versions involves the following steps: - the Master node distributes individual particles histories to the slave nodes which then assigns the tasks based on the number of threads running per node. Since the master-slave algorithm requires that each slave node possess its own problem data and geometry, the problem data and the collated tallies are communicated between slave and master nodes by message passing. The OpenMP is used for intra-thread communication on each node. Brown and Martin, (2004)

If there are no other computation tasks running on the Master node, the Master nodes await rendezvous at periodic intervals from the slaves, during this period, computation of histories is stopped and current tally is sent to the master. At the end of calculations, the slave nodes package the data and send them back to the Master node which then collates the results and produces the output. Deng and Xie, (1998)

MCNP is particularly suitable for parallel processing because the individual particle histories are independent such that there is no need to interchange data between slaves' nodes during computations and the fact that a compact 3D combinatorial geometry is employed such that no memory storage is needed for a large 3D mesh. Brown and Martin (2004)

To speed the calculation, we employed some parallel computing capabilities some of which is provided by default as binaries in the Windows version. In a Linux environment, the binaries are built using Intel FORTRAN compiler 12.1.5 version. In this work, we employed the MPICH2 version 1.4.1p1 as the parallel communication software.

MPICH is a portable implementation of the Message Passing Interface standard and it supports different computational and communication platforms including easily constructed. The software is distributed under an open source and free license and it is available on common platforms such as Windows, Linux, and Mac OS/X.

An IP network is configured allowing layer 3 communications between all the nodes that would participate in the calculation. Each of the nodes has the mpich software deployed IP network. The complete MCNP code with the data library is installed on the master computer, while the other nodes need only have the relevant MCNP binaries installed. On a Microsoft Windows platform, the computing environment is prepared to provide easy access to the executables and data files locations through PATH and DATAPATH environment variables. An equivalent procedure is carried out on other operating system platforms to enable ready access to the executable files.

The configuration of the systems used in this study is listed in Table 3-8 while Table 3-9 gives the result computer runtime for 430 cycles for different combinations of the number of cores and tasks while searching for an optimum system configuration to be used in the calculation.

Table 3-8 System configuration of nodes employed in the study

Name	Role	# Processors core	Processor Speed (GHz)	Memory (RAM) GB	Type of Processor
Dell1	Master with complete MCNP code installed	4	2.5	4GB	Intel core i5-3210
Dell2	Slave – binaries only	4	2.5	4GB	Intel core i5-3210
ENVY23	Slave – binaries only	4	3.3	16GB	Intel Core i3-3220 CPU
X6400 workstation	Slave – binaries only	2	2	2GB	Intel Xeon 5130
500MT	Slave – binaries only	2	3	4GB	Pentium Dual Core E5700
Pro3400a	Slave – binaries only	2	2.7	3GB	Intel Pentium G630
Pro3400b	Slave – binaries only	2	2.7	3GB	Intel Pentium G630

Table 3-9 Job runtime for different parallel computing system configurations

# of tasks	No of Cores	No of Systems	Average duration per cycle	Total Compute Time
16	4	4	1:02	7:24:20
12	4	3	1:20	9:33:20
19	4,4,4,4,3	5	1:30	10:45:00
21	4,4,4,3,3,3	6	1:20	9:33:20
8	4	2	1:50	13:08:20
4	4	1	3:56	28:11:20
4	1	4	1:57	13:58:30

Software Environment

Operating System: The operating system is a mix of Microsoft Windows Windows 7, Windows XP and Fedora Linux while the MCNP code is version mcnp5 v 1.60. The parallel communication software is mpich2 1.4.1p1. Other useful application includes Textpad and Teamviewer (for remote control, scheduling and job status monitoring)

The following applications, mpich, wmpiconfig, and wmpiexec are used to set up the hosts' computers giving the location of the working directory and the number of cores per hosts involved in the calculation. In this report, we used a cluster consisting of 7 hosts computers with a total of 20 cores.

4 RESULTS AND DISCUSSION

4.1 Fuel Properties

The multiplication factor of a critical assembly depends amongst other factors the enrichment and the fuel loading. The candidate LEU fuels were optimized to give an as-built excess reactivity of between 3.5mk and 4mk by varying the fuel meat density and limiting the volume percent of each fuel pin to a maximum of 40 vol. %. The volume fraction was chosen because it is a realistic value that can be produced for extruded pins dispersion fuels. Enrichment value for all the candidate LEU fuels was set at 19.75% thus necessitating that uranium densities greater than 5 g/cm^{3}would be needed to ensure that the fuel pin configuration of the reference HEU core design is maintained.

A direct substitution of the UAl_4 fuel pins with U_3Si_2-Al dispersion fuel of the same dimensions as an enrichment of 19.75% is shown in Matos and Lell (2005) to require a uranium density of 5.4 g/cm^3 to give the required excess reactivity. This density is beyond the 4.3 g/cm^3 corresponding to a 38 vol. %, hence a modification of the U_3Si_2 fuel pin is required. and this is done by altering the cladding thickness from 0.6mm to 0.38mm is needed to produce the required excess reactivity at a core loading of 1228g. This is comparable to the 1230.4g reported by Nawaz *et al* (2012)

A direct substitution of the HEU fuel with LEU U_3Si and U9Mo respectively indicate that no change in the fuel pin and cladding dimension is needed to achieve the same excess reactivity as the HEU fuel. The U9Mo fuel requires a density much greater than the U_3Si owing to comparatively higher neutron absorption cross of Molybdenum over Silicon. The core loading in this work for U_3Si and U9Mo are 1257g and 1361g respectively compared with 1251.8g and 1833.6 g reported by Nawaz *et al* (2012)

Our preliminary calculation shows that the optimized values for the three candidate LEU dispersion fuels is consistent with the feasibility study by Matos and Lell, (2005) and the results which are used in the subsequent calculations is presented in Table 4.1

Table 4-1 Fuel Material Properties of the Candidate LEU Fuels

	U_3Si-37.55% vol	**U_3Si_2-39.04% vol**	**U9Mo-38%vol**
Enrichment	19.75	19.75	19.75
Density of dispersed phase (g/cm^3)	15.20	12.20	17.20
Wt fraction of U in dispersed phase	0.96	0.93	0.91
Density of Meat (g/cm^3)	7.39	6.41	8.21
Mass loading of 235-U in meat (g)	3.62	3.54	3.92
Core loading 235-U (g)	1257.05	1228.06	1361.43
No of Pins	347	347	347
Fuel Meat outer diameter (mm)	4.30	4.74	4.30
Clad material/thickness (mm)	Al/0.6	Al/0.38	Al/0.6

4.2 Neutronics Properties

A full-core 3D modeling of the NIRR-1 core utilizing all the materials of the reactor was developed and validated using the MCNP5v1.6 code from which the effective multiplication factor k_{eff} and the neutron flux were obtained. The k_{eff} value from the MCNP code is derived from the combined collision, absorption and track-length estimators. The base calculations were carried out using a fresh core at 20°C. The defining card for determining k_{eff} in an MCNP criticality calculation is the KCODE card in the form

KCODE 500000 1.004 30 430

The card simulates a half a million particles in 430 cycles, 30 of these cycles are discarded to allow for the fission source to converge from the initial guess distribution and 1.004 is the initial guess of the k_{eff}. In this work, the number of fuel pins in the core, inner and outer

diameters of the core have been maintained at same dimensions as the HEU core for ease of comparison and so as not to change the thermal hydraulics considerations.

The result obtained for the HEU UAl_4 core is compared and benchmarked with data recorded at the zero-power experiment after which the data representing the candidate LEU fuels were simulated using the benchmarked model and the result obtained were then compared with feasibility work conducted by Jonah *et al* (2009) on the same reactor. The neutronics properties of control rod worth, shutdown margin etc. are determined by the effective multiplication factor. The simulation was done for different scenarios of the position of the central control rod ranging from completely withdrawn, completely inserted, and optimized critical position of the control rod where the k_{eff} value is near unity.

Core Excess Reactivity

The initial excess reactivity is defined as the core reactivity present when all control elements are completely withdrawn. It gives an indication of the fraction of neutrons in excess of that, which is required to keep the neutron population constant. Duderstadt and Hamilton, (1976). The daily operating time of the reactor is determined by the value of the initial excess reactivity at the start-up of the reactor. This value is also important as it determines the economy and the operational safety of the reactor and is given by

$$\rho_{ex} = \frac{k_{eff} - 1}{k_{eff}} \qquad 4.1$$

Control Rod Worth

The control rod worth is the reactivity worth of an individual control element and is given as change in core reactivity as a result of a full insertion of the rod. The MNSR has a single control rod, the justification of which is based on the inherent safety feature of the reactor.

$$\rho_w = \frac{k_{eff}^{out} - k_{eff}^{in}}{k_{eff}^{out} * k_{eff}^{in}} \quad 4.2$$

Shutdown Margin

The shutdown margin as given in Duderstadt and Hamilton, (1976) gives an indication of the core multiplication capability of the reactor core while the reactor is in a shutdown state. It also points to the rate at which power level may be reduced in an emergency. It is given by the expression below

$$\rho_w = \rho_{ex} + \rho_{sdm} \quad 4.3$$

Safety Reactivity Factor

The safety reactivity factor (SRF) is the ratio between the control rod worth and the core excess reactivity. Balogun *et al*, (2003), Dawahra *et al*, (2014)

$$SRF = \frac{\rho_w}{\rho_{ex}} \geq 1.5 \quad 4.4$$

The results of the Monte Carlo criticality calculation keff and basic reactor physics design parameters of core excess reactivity, control rod worth, shutdown margin and the safety reactivity factor for the HEU and the three dispersant LEU fuels cores are presented in Table 4.2 below.

Table 4-2 Measured and calculated core physics data of reference HEU and candidates LEU fuels

	HEU-UAl_4-90.2%(347) Measured	HEU $UAl_4$90.2% (347) Benchmarked	LEU-U_3Si 19.75% (347) Calculated	LEU-U_3Si2 19.75%(347) Calculated	LEU-U_9Mo 19.75%(347) Calculated
k_{eff} rod fully out		1.00475 ±0.00006	1.00472 ±0.00006	1.00478 ±0.00006	1.00482 ±0.00006
k_{eff} rod fully in		0.99715 ±0.00006	0.99799 ±0.00006	0.99807 ±0.00006	0.99829 ±0.00006
Unadjusted actual clean core excess reactivity, (mk) $\rho_{ex} = \frac{(k_{eff} - 1)}{k_{eff}}$	4.97	4.73	4.70	4.76	4.80
Adjusted Core Excess Reactivity (-1.2)mk	3.77	3.53	3.50	3.56	3.60
Control rod worth (mk) $\rho_w = \frac{(k_{eff}^{out} - k_{eff}^{in})}{(k_{eff}^{out} * k_{eff}^{in})}$	7	7.59	6.71	6.69	6.51
Shut Down Margin (mk)	3.33	4.06	3.21	3.13	2.91
Safety Reactivity Factor		2.15	1.92	1.88	1.81

The measured value of the cold core excess reactivity for the HEU core during the onsite start-up and zero power experiment was 4.97mk while the result by Jonah *et al* (2007) was 4.76±0.07 mk. The value of the unadjusted core excess reactivity from our model is 4.73+0.07 mk which compares favorably with both the measured value and previous work

done on the NIRR-1 core. It is noteworthy to state that the design recommendation for the clean cold core excess reactivity for the MNSR is between 3.5 and 4mk, hence it was necessary at startup to bring the measured reactivity of the NIRR-1 within the tolerance value by inserting a cadmium absorber of worth -1.2mk in one of the unconnected inner irradiation channels. It is evident that all the results for our candidate fuels obtained possess sufficient reactivity values to allow for the similar optimization.

The value of the control rod worth for the HEU core is 7.59 mk which is in close agreement with the measured value of 7.0 mk. The control rod worth for the LEU fuel configuration U_3Si, U_3Si_2 and U_9Mo are 6.71mk, 6.69 mk and 6.51 mk respectively close to the reported value by Nawaz *et al*, (2012) and Sampong *et al* (2006) of (6.041 mk and 6.586 mk for U_3Si) and (6.115 mk and 6.655 mk for U_3Si_2). The control rod worth is expectedly lower due to the higher ^{238}U in the LEU fuels thus a hardening of the neutron spectrum, hence there is a relative decrease in neutron flux near the center of the control rod thus lowering the neutron absorption. This is also evident in Figure 4.4 (a-c)

The reliability of the design employing the LEU fuels is compared with the experimental measurement and earlier feasibility studies. The shutdown margin obtained for the LEU fuels configuration are 3.21mk, 3.13mk and 2.91 mk for U_3Si, U_3Si_2 and U_9Mo respectively which is comparable to the experimental value of 3.33mk and the result obtained for the benchmarked HEU core of 4.06 mk.

It is observed that the safety reactivity factor for the candidate LEU fuels at 1.92mk, 1.88mk and 1.81mk for U_3Si, U_3Si_2 and U_9Mo respectively while lower than the result obtained for the HEU at 2.15mk are satisfactorily greater than the recommended SRF factor of 1.5 hence a modification of the control rod material and configuration is not required.

4.3 Coefficient of Reactivity

To determine the effect of fuel temperature on the reactivity, each of the cells representing the fuel region is amended using the TMP card expressed in eV which is an indication of the operating temperature of each fuel. The material card is taken from the appropriate evaluated nuclear data file. The factors contributing to the fuel temperature coefficient are Doppler broadening and the hardening of the spectrum.

In this work, the k_{eff} values were determined for fuel temperatures 293K, 400K, 500K and 600K respectively. For the moderator temperature coefficient, the temperature of the coolant in the reactor core is changed using the TMP card and the special hydrogen treatment for water is applied. The changes in reactivity are calculated for coolant temperatures at 293K, 313K, 333K, 343K 373K and 423K. the reference moderator temperature and density are chosen to be 293K and 0.99567g/cm^3 respectively.

Table 4-3 gives the result of the computation for the fuel, moderator and void coefficients of reactivity for the HEU fuel and the candidate LEU fuels. A comparison is made with the result for the HEU fuel by Jonah *et al* (2007) and Mahmood *et al* (2008).

Table 4-3 Coefficient of Reactivity

		UAl4	*UAl4 (Jonah et al -2007)*	*UAl4 (Mahmood et al 2008)*	U3Si	U3Si2	U9Mo
Fuel Temperature Coefficient (mk/K)	Temperature Range 293K - 600K	-9.28E-05			-8.04E-04	-9.08E-04	-7.31E-04
Moderator Temperature Coefficient (mk/ºC)	Temperature Range 20ºC - 150ºC	-6.15E-03	-5.37E-03	-6.53E-03	-3.37E-03	-3.99E-03	-3.04E-03
Moderator Density Coefficient (mk/ºC)	Corresponding to 20ºC - 100ºC	-3.64E-01	-3.65E-01	-3.38E-01	-3.58E-01	-3.65E-01	-3.71E-01

The contribution to the reactivity feedback is greatest for the void when compared to the fuel and moderator heating. The result indicates that there is an increasingly negative contribution to reactivity as coolant temperature increase. It is observed that the average fuel coefficient of reactivity increased reactivity from -9.28 x 10^{-5}mk/K for UAl_4 to -8.04 x 10^{-4} mk/K, -9.08 x 10^{-4}mk/K and -7.31x 10^{-4}mk/K for U_3Si, U_3Si_2, and U_9Mo respectively, this is attributed to the increased ^{238}U content in the LEU fuels. The void coefficient contribution is simulated by changing the density of the coolant water and assuming a correlation between the void fraction and moderator density. The simulation was performed for coolant water densities according to the John Stillman data in Table 4-4.

Table 4-4 John Stillman's Data Based on CRC Handbook at 1 atm

Mod-Temp, C	Density	% Void
20C	0.99825	ref
30C	0.99567	-0.26
50C	0.98807	-1.02
60C	0.98324	-1.50
100C	0.95838	-3.99
~165C	0.89843	-10.00
~250C	0.79860	-20.00

Figures 4-1 to 4-3 gives the variation of reactivity as a function of fuel temperature, moderator temperature and moderator density for HEU-UAl_4 and LEU-U_3Si, LEU-U_3Si_2 and LEU-U9Mo.

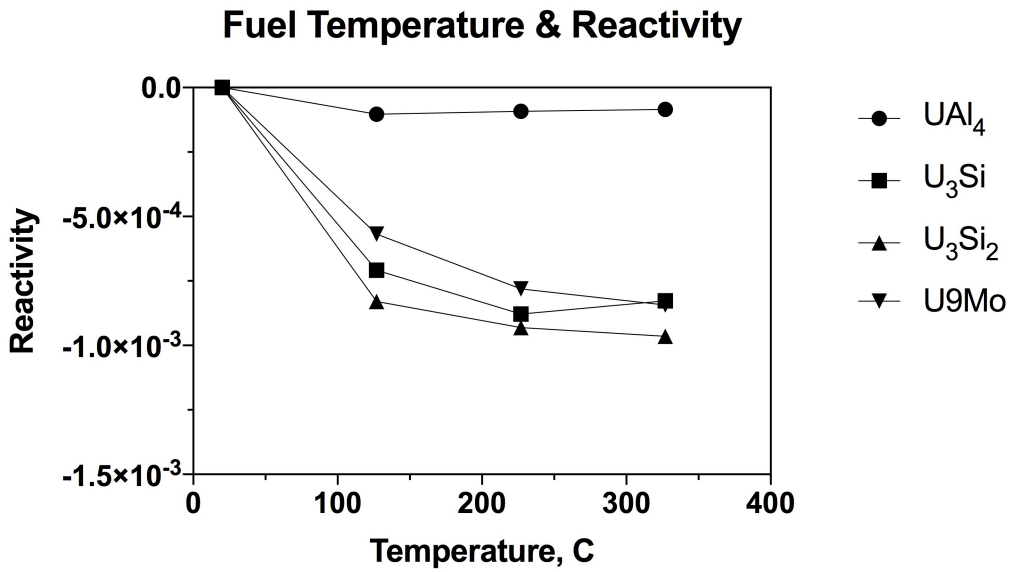


Figure 4-1 Dependence of reactivity on Fuel Temperature

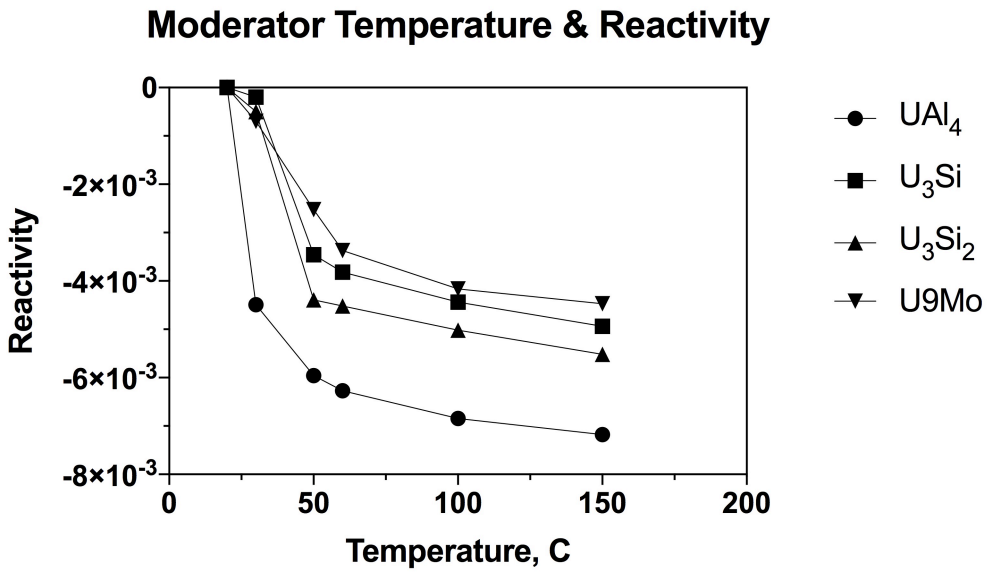


Figure 4-2 Dependence of reactivity on Moderator Temperature

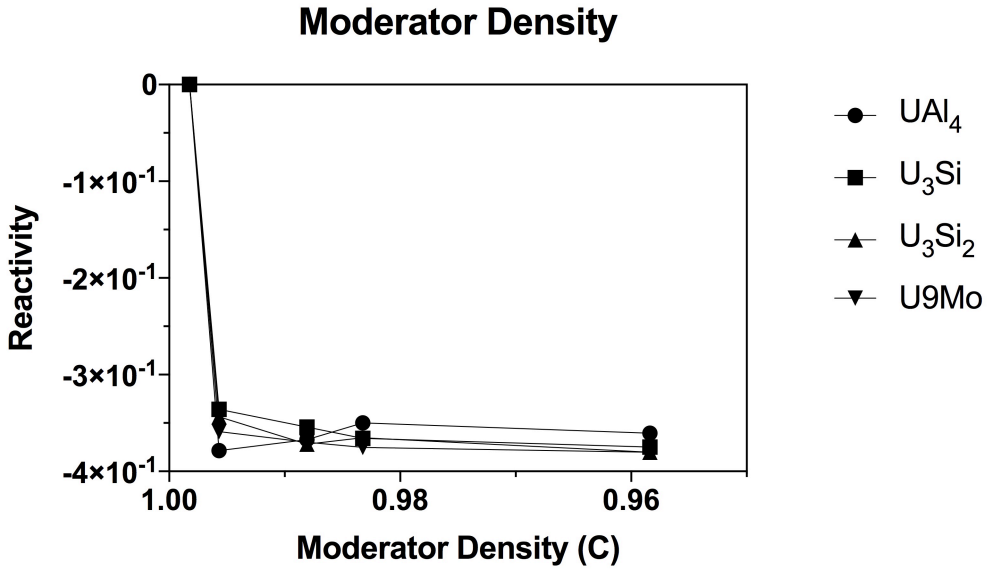


Figure 4-3 Dependence of reactivity on Moderator Density

4.4 Flux Distribution

The MCNP has been demonstrated for the criticality calculations of core physics parameters such as k-effective eigenvalues, kinetic parameters, and neutron flux and spectrum and power distribution. However, the values in the MCNP outputs obtained with the tally cards (F4 and F7 for flux and power respectively) are relative values and needs to

be normalized based on the operating power. This is due to the fact that for KCODE calculations, the flux output in the mctal files is un-normalized with the assumption of one-fission source neutrons, hence the average number of neutrons released per fission must be taken into consideration. The normalized fluxes are obtained by multiplying by the scaling factor.

The scaling is

$$S = \frac{P\bar{v}}{(1.6022 \times 10^{-13}) \cdot w_f k_{eff}} \qquad 4.5$$

where P is the thermal power in Watts, w_f is the effective energy released per fission in MeV and v is the average number of neutrons released per fission. The F4 tally of the code was used to calculate the axial thermal, epithermal and fast neutron flux distribution in the inner and outer irradiation channels, the fission chamber and the slant tube using a 3-group energy treatment with the following group energy boundaries given as thermal (0-0.625eV), epithermal (0.625eV-0.825MeV) and fast (0.825MeV to 20MeV). The inner and outer channels are located at a radial distance of 16.5 cm and 24.5 from the center of the core and ten axial segments were used to tallying scores in the irradiation channels, fission chamber and the slant tube. The calculated neutron fluxes for the inner and outer irradiation sites are given in Table 4-5 and Table 4-6 shows the neutron fluxes for the fission chamber and the slant tube respectively. The conversion factor was used to normalize the criticality calculation to the steady-state power level of the reactor at 31kW.

Table 4-5 Calculated thermal, epithermal and fast flux in the inner and outer irradiation sites

Neutron Energy/Fuel Type	Thermal (0-0.625eV) n/cm^2.s x10^{11}		Epithermal (0.625eV-0.825MeV) n/cm^2.s x10^{11}		Fast (0.825MeV to 20MeV) n/cm^2.s x10^{11}	
Location	Inner	Outer	Inner	Outer	Inner	Outer
HEU-UAl_4	11.57±01	6.60±01	12.96±01	1.85±01	2.69±01	0.361±003
LEU-U_3Si	10.73±01	6.34±01	12.83±01	1.83±01	2.64±01	0.354±003
LEU-U_3Si_2	10.69±01	7.17±01	12.83±01	2.07±01	2.65±01	0.403±003
LEU-U_9Mo	10.47±01	7.10±01	12.78±01	2.07±01	2.63±01	0.401±003

Table 4-6 Calculated thermal, epithermal and fast flux in the fission chamber and the slant tube

Neutron Energy/Fuel Type	Thermal (0-0.625eV) n/cm^2.s x10^{11}		Epithermal (0.625eV-0.825MeV) n/cm^2.s x10^{11}		Fast (0.825MeV to 20MeV) n/cm^2.s x10^{11}	
Location	Fission Chamber	Slant Tube	Fission Chamber	Slant Tube	Fission Chamber	Slant Tube
HEU-UAl_4	11.85±01	0.252±002	13.13±01	0.036±005	2.60±01	0.0184±0004
LEU-U_3Si	11.02±01	0.248±002	12.97±01	0.035±005	2.52±01	0.0173±0004
LEU-U_3Si_2	11.00±01	0.252±002	13.02±01	0.035±005	2.54±01	0.0175±0004
LEU-U_9Mo	10.75±01	0.246±002	13.00±01	0.035±005	2.52±01	0.0176±0004

The relative difference in the thermal flux between the HEU fuel configuration and the LEU fuels U_3Si, U_3Si_2 and U_9Mo simulated at a reactor power level of 31 kW shows a percentage decrease of 7.3%, 7.6% and 9.5% in the inner irradiation channel. A similar depression in flux levels was observed in the fission chamber for the LEU fuels. The inner irradiation channel and the fission chambers are at the same radial distance from the center of the core and at the similar depth of immersion in the beryllium annulus hence the thermal fluxes obtained in this calculation for the inner irradiation channels and the fission

chamber are 11.57 n/cm^2.s x10^{11} and 11.85 n/cm^2.s x10^{11} which is consistent with 11.6 n/cm^2.s x10^{11} and 11.9 n/cm^2.s x10^{11}reported by Liaw and Matos (2007).

The ratio of the thermal/epithermal and thermal/flux neutron flux in the inner irradiation channel is given in Table 4-7. The values are in close agreement with the reported ratios for the Canadian SLOWPOKE-2 an MNSR type reactor Kennedy *et al* (2002) in which the thermal/fast ratio dropped from 4.4 for the HEU core to 4.0 for the LEU-UO2 core.

Table 4-7 Flux Ratios in the Inner Irradiation Site

MCNP Channel	UAl4	U3Si	U3Si2	U_9Mo
Thermal/Epithermal Flux Ratio	0.89	0.83	0.83	0.82
Thermal/Fast Flux Ratio	4.30	4.06	4.03	3.98

In the outer irradiation channels, the thermal neutron flux obtained for the HEU core is 6.60±01 n/cm^2.s x10^{11} which is about half the value for the inner irradiation channel at 11.57±01 n/cm^2.s x10^{11}.

Table 4-8 gives a comparison between the thermal flux levels in the five inner irradiation channels for 3 fuel configurations, the original HEU-UAl_4 core at 31 kW, LEU-U_3Si core at 31kW and LEU-U_3Si core at 34kW

Table 4-8 Peak flux in the inner irradiation channels in n/cm2.s for HEU and candidate LEU -U3Si

MCNP Channel	HEU-UAl4 31kW (n/cm^2.s)	LEU-U3Si 31kW (n/cm^2.s)	LEU-U3Si 34kW (n/cm^2.s)
Cell 971	1.16227E+12	1.07830E+12	1.22208E+12
Cell 933	1.15182E+12	1.06955E+12	1.21216E+12
Cell 935	1.15365E+12	1.06724E+12	1.20954E+12
Cell 937	1.17183E+12	1.08678E+12	1.23169E+12
Cell 939	1.14173E+12	1.06305E+12	1.20479E+12
Average	1.15704E+12	1.07299E+12	1.21605E+12

Comparison of axial thermal flux in inner irradiation channels exhibits similar patterns except for slight depression in flux between 7% and 10% due to spectrum hardening of the LEU fuels. This is similar to the decrease by 6% - 7% reported by Albarhoum (2011) for U_3Si_2 fuel. It is also observed in Figure 4-4 that the gradient of the calculated thermal neutron flux in the irradiation channel around the middle of the fuel pin does not exceed the 3% recommended in the safety analysis report FSAR (2005) implying an axial thermal flux distribution suitable for NAA. It is evident from the calculations with the candidate LEU fuels that the safety of the reactor is not compromised if core configurations remain the same. In addition, the utilization of the NIRR-1 reactor for neutron activation analysis is not affected since the thermal neutron flux obtained for all the fuels are within 10% of the rated flux for the reference HEU core. It is however necessary to raise the power level of the reactor from 31 kW to increase to 33.3 kW, 32.4 kW and 33.9 kW for U_3Si, U_3Si_2, and U_9Mo respectively to match the nominal power flux level in the inner irradiation sites for the HEU core.

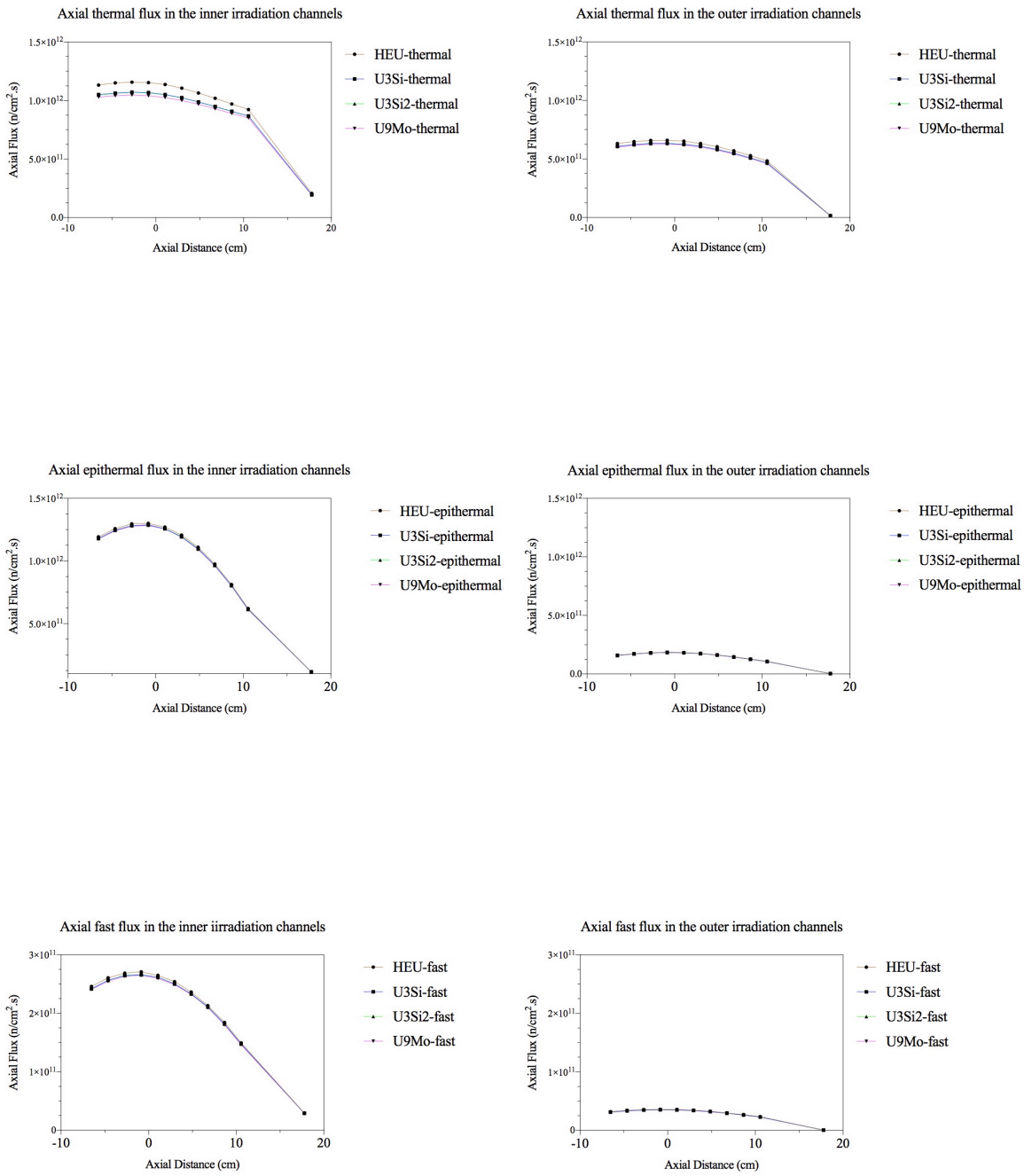


Figure 4-4 Axial thermal flux distribution for HEU and Candidate LEU fuels in the inner and outer irradiation channels

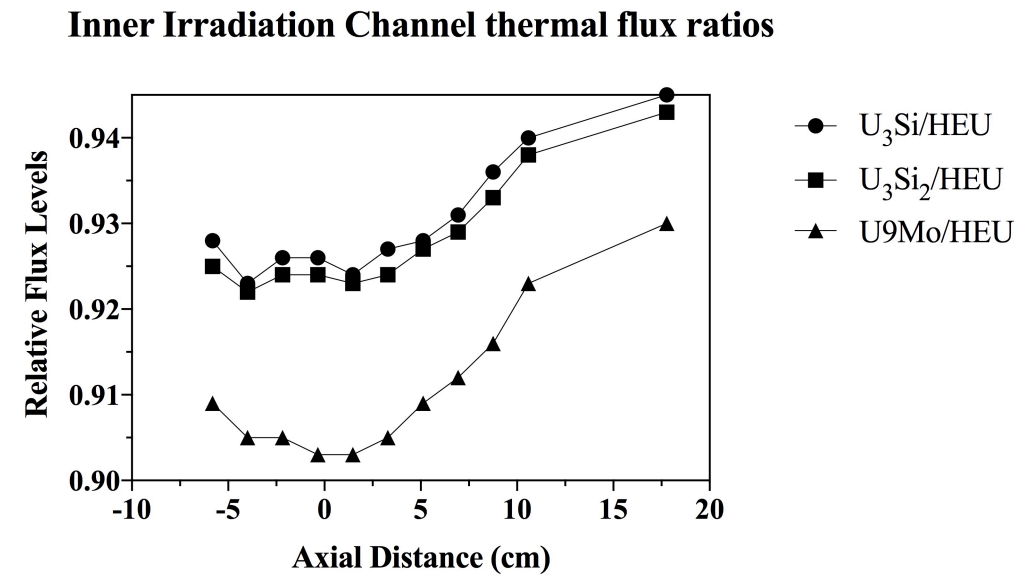


Figure 4-5 Thermal flux ratio HEU with candidate LEU fuels in a selected inner irradiation channel

Figure 4-5 compares the thermal flux levels in the inner irradiation channel for the reference HEU core and the cores using the candidate LEU fuels and it is observed that the thermal flux level for U_3Si core more closest to that of the reference HEU core.

Figure 4-6 gives the axial thermal, epithermal and fast neutron flux distributions for the HEU-UAl4 and the LEU fuels U_3Si, U_3Si_2 and U9Mo in the inner irradiation channels. It is observed that the inner irradiation channel shows a higher epithermal flux levels for all the candidate LEU fuels and this is because the inner irradiation channel being very close to the core where fast neutrons born from fission do not travel sufficiently great distance before reaching the inner irradiation channels, hence they do not suffer enough collision to bring the neutrons to thermal energies.

Owing to the depressed flux from the use of LEU fuels, there is the need to increase the operating power to match the flux level of the HEU core, the effect of increasing operating power for each of the candidate LEU fuels is presented Figure 4-7.

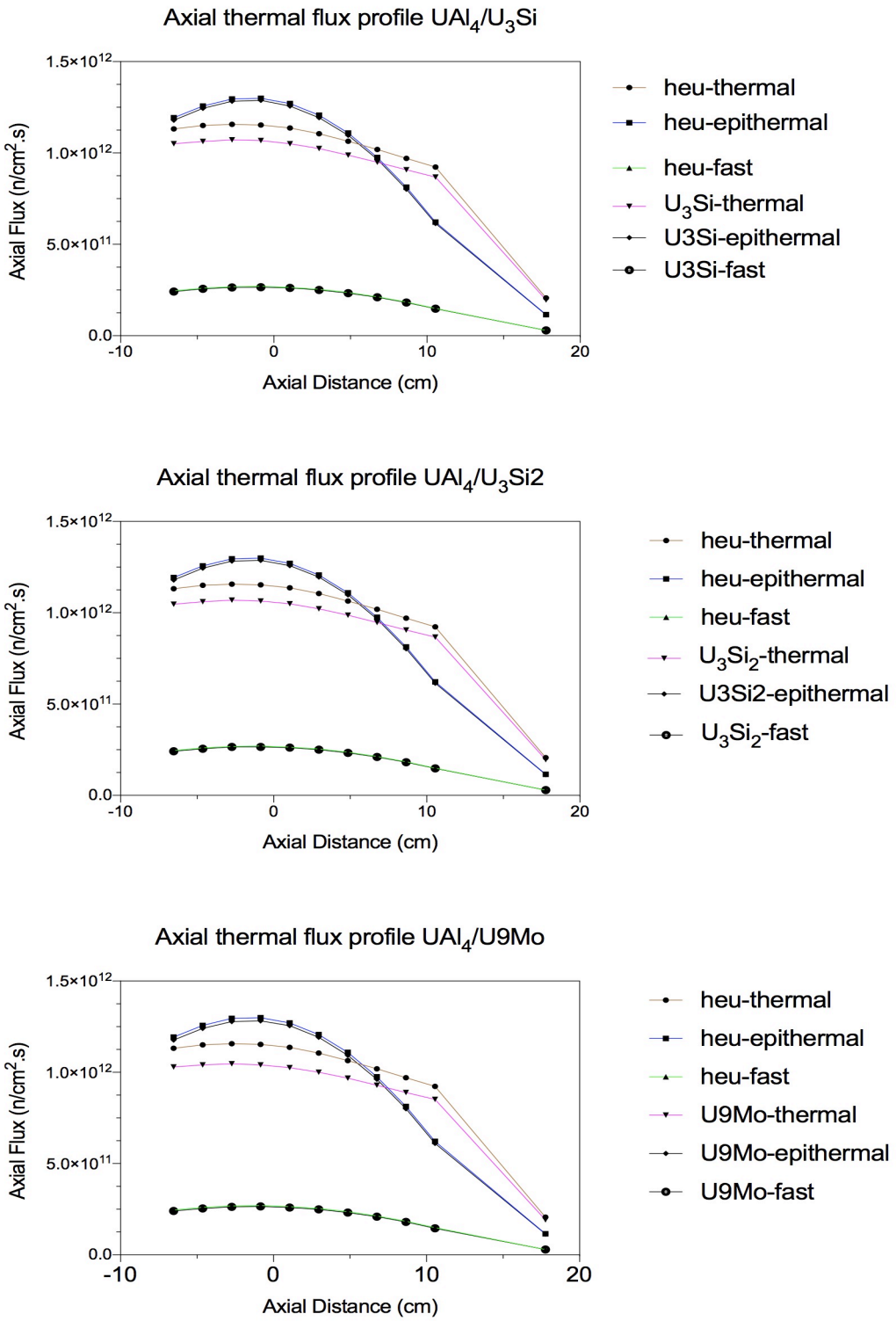


Figure 4-6 Comparison of axial thermal, epithermal and fast flux for the HEU and LEU fuels in the inner irradiation channel

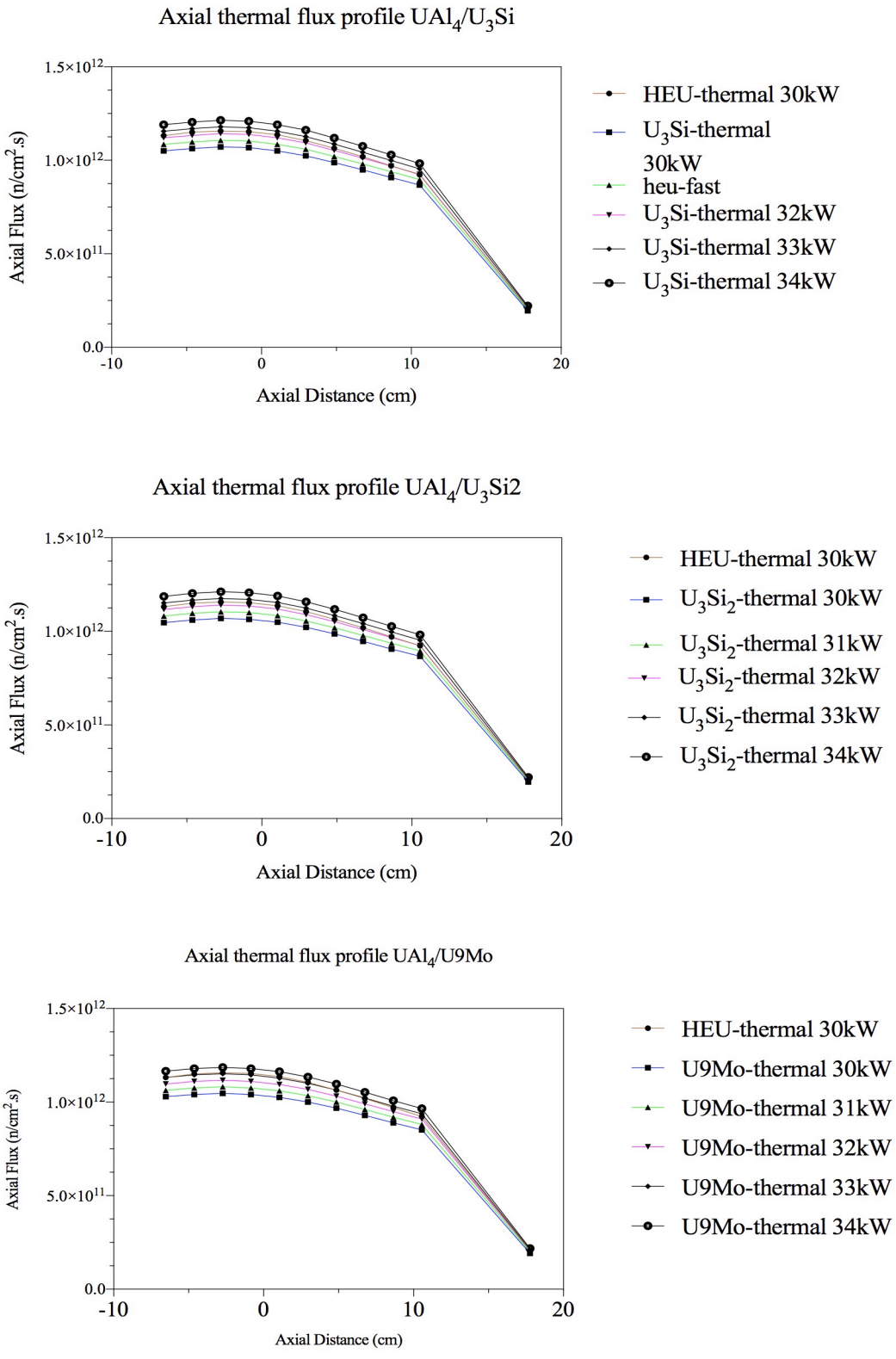


Figure 4-7 Axial thermal neutron flux distribution as a function of operating power

Figure 4-8 gives the axial thermal neutron flux distribution for U_9Mo when the moderator temperature is changed from between 20°C and 60°C. It is evident that the neutron flux distribution is not altered appreciably as the moderator temperature changes during a normal daily operating temperature range. This is consistent with the result observed by Khattab *et al* (2006) for the Syrian MNSR using the WIMSD and CITATION codes.

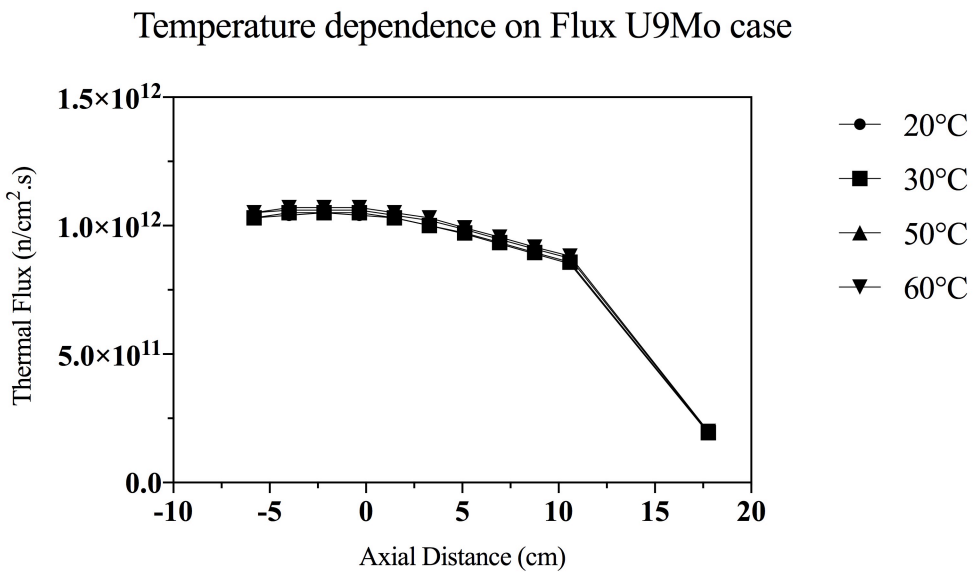


Figure 4-8 Axial Thermal Neutron Flux distribution for different moderator temperatures

4.5 Kinetic Parameters

In this work, we determined the effective delayed neutron fraction β_{eff} using two methods: TOTNU card and a new feature in MCNP5 v1.6 code – KOPTS card. The default run of the MCNP assumes the use of all neutrons (prompt and delayed in the calculation which is represented explicitly by the TOTNU YES. Turning off the TOTNU card by TOTNU no enables the calculation of the effective delayed neutron fraction.

The KOPTS adjoint flux method also enables the determination of the prompt neutron lifetime l_p. The result of the analyses of β_{eff} and the l_p with their associated uncertainties

from MCNP run for the HEU and the candidate LEU fuels are presented in Table 4.9 below.

Table 4-9 Comparison of kinetics data of LEU fuels with data for the HEU core

Kinetic Parameters	CIAE (quoted values)	HEU 90% (347)	LEU U_3Si 19.75% (347)	LEU U_3Si_2 19.75% (347)	LEU-U_9Mo 19.75% (347)
β_{eff} (TOTNU)	0.0081	0.00834±0.00008	0.00831±0.00008	0.00841±0.00008	0.00836±0.00008
β_{eff} (KOPTS)	0.0081	0.00849±0.00008	0.00840±0.00008	0.00843±0.00008	0.00844±0.00008
l_f (KOPTS) (μs)	81.2	56.09±0.09	50.33±0.09	50.21±0.09	48.71±0.09

The value of β_{eff} for the HEU core 0.00834 is comparable with the experimental result reported by the reactor manufacturers 0.0081. It is noted that effective delayed neutron fraction is largely unaffected by the choice of the fuels which is consistent with the result presented by Snoj *et al* (2010)

The result of the prompt neutron lifetime for the HEU fuel 56.09μs is of the same order of magnitude as the quoted value of 81μs by the reactor manufacturers and is in good agreement with the result using the 1/v insertion method reported by Jonah *et al* (2007) of 57.9 μs. and Khattab and Suleiman, (2011) of 54.9μs for the Syrian MNSR. The result also indicates a decrease in the value of the prompt neutron lifetime for the candidate LEU fuels which is attributable to hardened neutron spectrum due to higher U^{238} content. This is consistent with the result reported by Jonah and Ibikunle (2009) and Odoi *et al* (2014). The greater value of the delayed neutron fraction is a result as it allows adequate time for reactor operator control and safety.

4.6 Power Distribution

One of the features of the MCNP code is the capability of generating the axial power profile of the fuel pins in the reactor core. This is useful in thermal hydraulics calculations. Figure 4-9 compares the HEU core peak power to each of the candidate LEU cores.

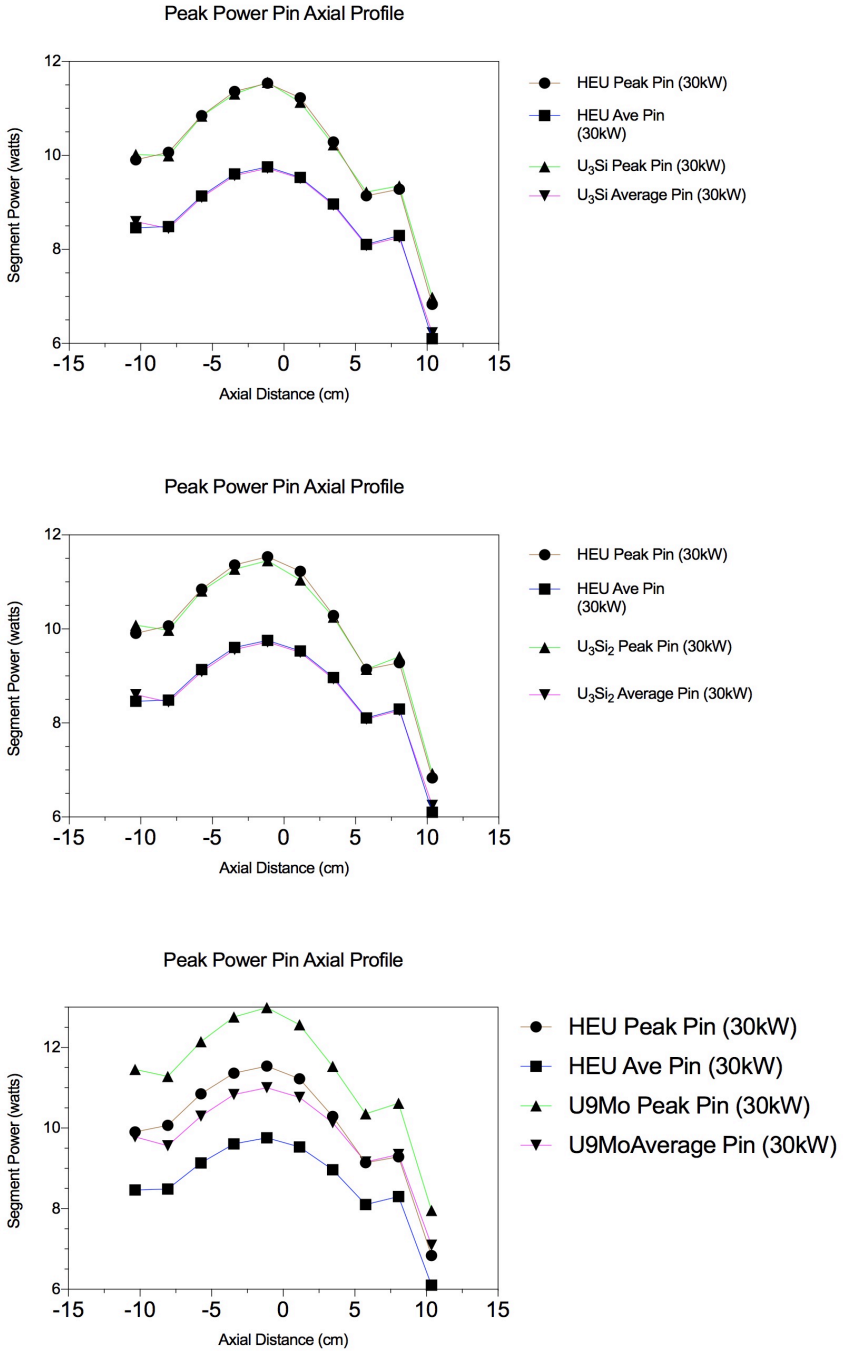


Figure 4-9 Peak Power Axial Profile

Figure 4-10 compares the computed power peaking factors for the HEU core and the candidate LEU cores. The plot agrees with the result by Bokhari and Pervez (2010)

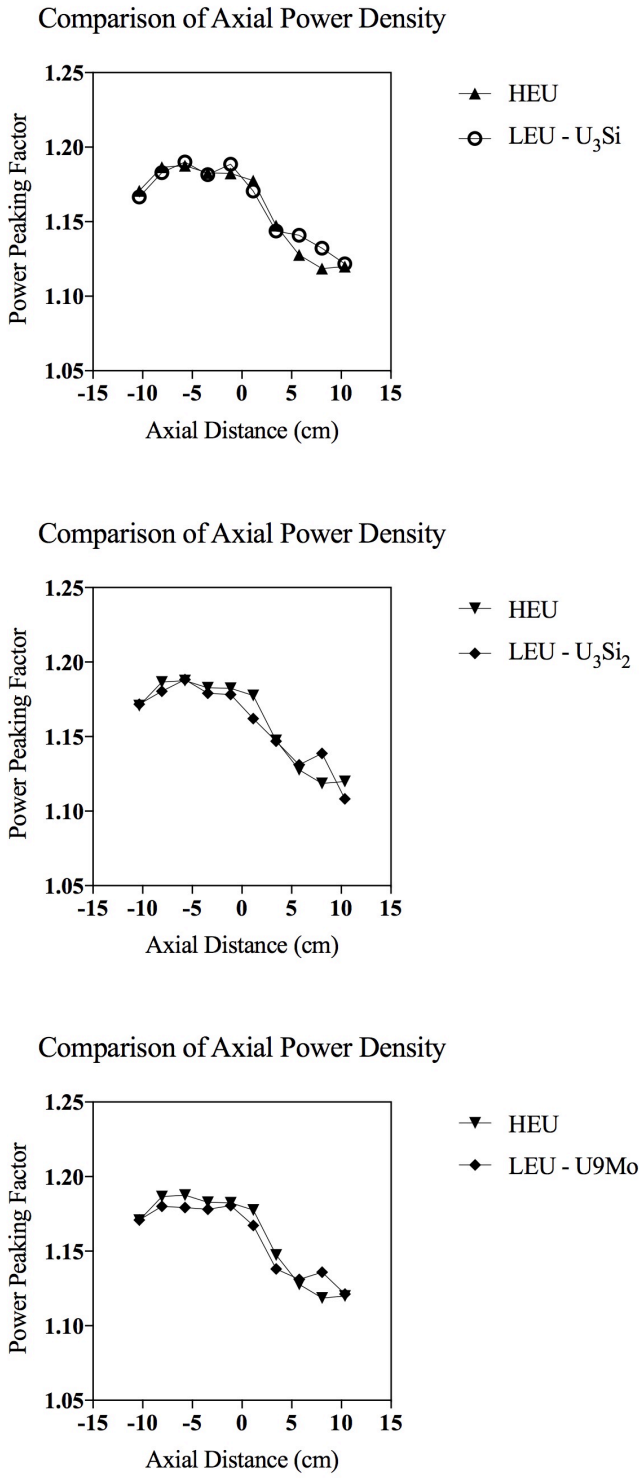


Figure 4-10 Comparison of the Power Peaking Factors for HEU core and LEU cores

5 SUMMARY, CONCLUSIONS AND RECOMMENDATIONS

5.1 Summary and Conclusion

An MCNP 3D Model of the current HEU core was established and successfully benchmarked with the basic core physics parameters of effective multiplication factor, core excess reactivity, control rod worth, shutdown margin, safety reactivity factor, reactivity coefficients and kinetic parameters obtained from experiment. Good agreement was also obtained with results from other researchers. The model was now extended to cover the following candidate LEU dispersion fuels U_3Si, U_3Si_2 and U9Mo.

Calculations involving the optimization of the uranium densities, volume fractions and uranium enrichments of the LEU candidate fuels were carried to determine the combination of values that matched the excess reactivity for the clean cold HEU core.

The core physics parameters of effective multiplication factor, core excess reactivity, control rod worth, shutdown margin, safety reactivity factors were calculated for the 3-D whole core MCNP model of the NIRR-1 using the proposed dispersion LEU fuels, results obtained are in good agreement with literature and with the current HEU. The result for safety reactivity factor shows that all the candidate LEU fuels are within the recommended values of > 1.5 and the coefficients of reactivity under changes in fuel temperature, moderator temperature, and moderator density confirms the inherently safe nature of the MNSR. The moderator density coefficient has the most dominant contribution in all the dispersion fuels studied. The prompt neutron lifetime is shorter in all the candidate LEU fuels compared with the HEU fuel owing to fuel Doppler effect. There was good agreement in results obtained for effective delayed neutron fraction using both KOPTS adjoint flux and TOTNU methods. The flux and spectra values in the irradiation sites, fission chamber

and slant tubes were calculated and the results shows a depressed flux levels compared to the flux levels in the HEU core, thus implying the need to increase the reactor power from 31 kW to increase to 33.3 kW, 32.4 kW and 33.9 kW for U_3Si, U_3Si_2, and U9Mo respectively, to match the nominal flux level in the inner irradiation sites for the HEU core.

The NIRR-1 model using the MCNP transport code has been extended for the candidate dispersion fuels and the results show that the NIRR-1 reactor may be successfully converted from the current HEU-UAl_4 fuel to LEU using any of the three fuel options studied in this work. In the case of the U_3Si2 fuel, it was necessary to alter the fuel pin diameter and the clad thickness to achieve the required excess reactivity.

Recommendations

A suggested extension of this study is to carry out safety analyses and thermal hydraulics calculations to determine the maximum centerline fuel temperatures for each of the LEU dispersion fuel options. The values of the peak power, fuel, clad and coolant temperatures due to reactivity insertions would then be calculated for the LEU candidate fuel options.

Safety analyses studies would be conducted to ensure that safety margins obtained for the U_3Si_2-Al, U_3Si-Al and U_9Mo-Al LEU fuels under normal daily operation and accident conditions would match or surpass the existing HEU core safety parameters.

A review of accident initiators in the HEU FSAR should also be conducted to determine changes that would be required owing to the use of the proposed LEU dispersion fuels.

An exploratory study of the radionuclide inventory via reactor burnup calculations for each of the fuel options is recommended to provide a basis for future core replacement.

REFERENCES

Abtin, F., Feghhi, S. A. H., Jafarakia, S., 2013. Neutronic evaluations for MNSR research reactor core conversion from HEU to LEU. *Annals of Nuclear Energy* 51: 69 – 73.

Albarhoum M 2011. The Use of U_3Si_2 dispersed fuel in Low-power research reactors. *Annals of Nuclear Energy* 39, pp 1206-1210

Albarhoum M 2011. Invariability of neutron flux in internal and external irradiation sites in MNSRs for both HEU and LEU cores. *Indian Journal of Pure and Applied Physics* 49. February 2011, pp 83 -90

Aldawahra S, Khattab K and Saba G, 2015. Neutronic analysis for core conversion (HEU-LEU) of the low power research reactor using the MCNP4C code. *Nukleonic* Vol. 60 (2) pp 367 – 371

Anderson, H. L. 1986. Metropolis, Monte Carlo and the MANIAC. *Los Alamos Science*, Fall Edition

Anim-Sampong S, Maakuu B.T, Akaho E.H.K, Andam A, Law J. J. R and Matos J. E (2006). "Progress in the Neutronic Core Conversion of Ghana Research Reactor". Paper Presented at the International Meeting on Reduced Enrichment for Research and Test Reactors (RERTR); Cape Town, South Africa (South Africa); 29 Oct - 2 Nov 2006

Azande, T. S., Balogun, G. I., Ajuji, A. S., Jonah, S. A., Ahmed, Y. A., 2010. The Use of WIMS and CITATION Codes in Fuel Loading Required for the Conversion of MNSR HEU Core to LEU. *Annals of Nuclear Energy,* 37 pg. 1223-1228.

Azmy, Y and Sartori, E. 2010. *Nuclear Computation Science: A Century in Review*, Springer Science + Business Media, B. V.

Bell, G. I. and Glasstone S. 1970 *"Nuclear Reactor Theory"*, Van Nostrand Reinhold Company

Bokhari, I. H., Pervez, S., 2010. Safety Analysis for Conversion (from HEU to LEU) of Pakistan Research Reactor – 2 (PAAR-2). *Nuclear Engineering and Design*, 240: 123 – 128.

Bretscher, M. M., 1997. Perturbation-independent Methods for Calculating Research Reactor Kinetic Parameters. Reduced Enrichment for Research and Test Reactors Program, ANL/RERTR/TM-30, Argonne, USA.

Brown, F. B. 2002. "MCNP Version 5" LA-UR-02-3935 submitted to the American Nuclear Society, 2002 Winter Meeting, November 17-21, Washington, DC

Brown, F. B. 2007. "The MCNP5 Random Number Generator", LA-UR-07-7961

Brown, F. B. 2009 “A review of Monte Carlo Criticality Calculations” International Conference on Mathematics, *Computational Methods and Reactor Physics* (MandC 2009)

Brown, F. B. 2009 “A review of Best Practices for Monte Carlo Criticality Calculations” American Nuclear Society, Nuclear Criticality Safety Topical Meeting.LA-UR-09-3136

Brown, F. B., Martin, W. R., 1984. Monte Carlo Methods for Radiation Transport Analysis on Vector Computers. *Progress in Nuclear Energy*, Vol. 14, No. 3,

Brown, F. B., Martin, W. R., 2004. High Performance Computing and Monte Carlo. *American Nuclear Society,* 2004 Winter Meeting at Washington DC November 14 - 18

Damn G, Nabbi R, 2002. Status of HEU-LEU Conversion of FRJ-2. Paper presented at the International Meeting on Reduced Enrichment for Research and Test Reactors held at Sancarlos de Bariloche, Argentina,3-8November.

Dawahra S., Khattab, K and Saba G. (2016) Reactivity coefficients for the HEU and LEU fuel of the MNSR reactor. *Progress in Nuclear Energy*, 88, pp 28 - 32

Deng, Li and Xie, Zhong-Sheng (1999) “Parallelization of the Monte Carlo Neutron and Photon Transport Code in Parallel Virtual Machine and Message Passing Interface” *Journal of Nuclear Science and Technology*, Vol. 36 No. 7 pp. 626-629

Dunn W. L. and Shultis, J. K. (2012) Exploring Monte Carlo Methods, Elsevier, Academic Press, Burlington, MA

FSAR (2005). Final Safety Analysis Report of Nigeria Research Reactor-1, CERT Technical Report - CERT/NIRR-1/FSAR-01.

Fisher, H. M. 1989. *A Nuclear Cross-Section Data Handbook*, LA-11711-M, Los Alamos National Laboratory, USA

Glaser. A, 2005. About the Enrichment Limits for Research Reactor Conversion: Why 20%? Paper Presented at the 27th International Meeting on Reduced Enrichment for Research and Test Reactors (RERTR) Boston, Massachusetts, 6 – 10, November

Guotu, K, Ziyong S, Feng F, Tiancai L, Yiguo L and Yongmao Z. (2009) The Study of Physics and Thermal Characteristics for In-Hospital Neutron Irradiator (INHI). *Applied Radiation and Isotopes* 67, pp. S234-S237.

Hammersley J.M. and Handscomb D.C. (1964) Monte Carlo methods. *Monographs on Statistics and Applied Probability*. 1st Edition. Springer Netherland publishing

Hanan, N. A., Pond, R. B., and Matos J. E. Matos, (2002) “Revisiting the Hfr-Petten LEU Conversion Study” Proceedings of the International Meeting on Reduced Enrichment for Research and Test Reactors, San Carlos de Bariloche, Argentina, November 3-8, 2002

Hainoun, A. Hassan H. and Ghazi N. (2009) "Determination of major kinetic parameters of the Syrian MNSR for different fuel loading using Monte Carlo technique" *Annals of Nuclear Energy* Vol. 36 pp. 1663 - 1667

Hanson A.L and Diamond D.J 2012, Calculations of the Kinetics Parameters for the NBSR. A Manuscript prepared for the Nuclear Science and Technology Department, Brookhaven National Laboratory, US Department of Energy, National Nuclear Security Administration BNL-97002-2012

Hanson A.L and Diamond D.J 2012, Prompt Neutron Lifetime for the NBSR Reactor, Transactions of the American Nuclear Society, Vol. 106, Chicago, Illinois, June 24 -28

Holden, A.N 1967, *Dispersion Fuel Elements*, Gordon and Breach Science Publishers, Inc., New York

Huda, M.Q., Rahman, M., Sarker, M.M., Bhuiyan, S.I., 2004.Benchmark analysis of the TRIGA MARK II research reactor using Monte Carlo techniques. *Annals of Nuclear Energy* 31, pp. 1299–1313

IAEA-Tecdoc-384 1985 "Technology and use of Low Power Research Reactors" Report of a Consultants meeting on the technology and use of low power research reactors organized by IAEA, Beijing China 30 April – 3 May 1985

IAEA, 1978. IAEA During International Nuclear Fuel Cycle Evaluation (INFCE, 1978-80)

Irving, D. C. 1971. The Adjoint Boltzmann Equation and its Simulation by Monte Carlo, *Nuclear Engineering and Design* 15, 273 - 292

Jonah S, Liaw J. R., Olson A, Matos JE 2006 Criticality calculations and transient analysis of the Nigeria MNSR (NIRR-1) for conversion to LEU. "Proceedings of the 28th International Meeting on Reduced Enrichment for Research and Test Reactors (RERTR) Cape Town" October 29 – November 2

Jonah S. A., Balogun G. I., Umar I. M., Mayaki, M. C., 2005. Neutron spectrum parameters in irradiation channels of the Nigerian Research Reactor-1 for the k_o-NAA standardization, *Journal of Radio-analytical Nuclear Chemistry*. 266, pp. 83-88.

Jonah S. A., Ibikunle K, Li Y., 2009. A Feasibility Study of LEU Enrichment Uranium fuels for MNSR conversion using MCNP. *Annals of Nuclear Energy* 36, pp. 1285-1286.

Jonah S. A., Ibrahim V. Y., Akaho E. H. K., 2008. The determination of reactor neutron spectrum Averaged Cross-section Using Miniature Neutron Source Facility. *Applied Radiation Isotopes* 66, pp. 1377-1380.

Jonah S. A., Liaw J. R., Matos J. E., 2007. Monte Carlo Simulation of Core Physics Parameters of Nigerian Research Reactor-1. *Annals of Nuclear Energy* 34, pp. 953-957.

Jonah S.A., Ibikunle K., Liaw J.R., Olson A., Matos J.E., 2006. Neutronics Parameters and Transient Analysis of the NIRR-1 for conversion to LEU. Paper presented at the 1st IAEA-CRP Conversion of MNSR to LEU, Vienna, Austria, 11-14 December.

Jonah, S. A., 2011. Measured and simulated reactivity insertion transient Characteristics of NIRR-1. *Annals of Nuclear Energy*, 38 pp. 295 - 297

Kalos M. H and Whitlock P. A. (2008) *Monte Carlo Methods*. Wiley Blackwell Publishing, Second Revised Edition

Ke, G., Sun, Z., Shen, F., Liu T, Li Y., Zhou, Y., 2009. The Study of Physics and Thermal Characteristics for in-hospital neutron irradiator (INHI). *Applied Radiation and Isotopes* 67, pp. S234-S237.

Kennedy G, St Pierr, J., Benner I. G. I., Nielsen K. S., 2002. Low-fueled SLOWPOKE-2 research reactors; Operational experience and utilization. Proceedings of the 2002 International meetings on Reduced Enrichment for Research and Test reactors Bariloche, Argentina November 3 – 8

Kelvin, L. (1901) Nineteenth century clouds over the dynamical theory of heat and light. *Philosophical Magazine*, Series 6, 2, 1.

Khattab K., Suleiman, I., 2011 Monte Carlo simulation of core physics parameters of the Syrian MNSR reactor. *Annals of Nuclear Energy* 38, pp. 1211-1213.

Khattab, K. and Suleiman I., 2009 Assessment of fuel conversion from HEU to LEU in the Syrian MNSR reactor using the MCNP code. *Progress in Nuclear Energy* 51 pp. 727 – 730

Kiedrowski B.C., Booth T.E., Brown F.B, Bull J.S. Favorite J.A., Forster R.A., and Martz R.L. MCNP5-1.60: Feature Enhancements and Manual Clarifications, LA-UR-10-06127, X-Computational Physics Division, Los Alamos National Laboratory.

Kim C., Jang S. and Reece W. D. (2004) "Monte Carlo Modeling of the Texas A&M University Research Reactor" *Nuclear Technology* Vol. 145 , Iss. 1, pp. 1 – 10

Landers. C, 2005. Reactors Identified for Conversion, a paper presented at the International meeting on Reduced Enrichment for Research and Test Reactors, November 6 – 10, Boston, Massachusetts.

Lamarsh, J. R. (1972). *Introduction to Nuclear Reactor Theory*, Addison Wesley Publishing Company

Lehmer, D.H. (1951), "Mathematical Methods in Large-Scale Computing Units," *Annu. Comput. Lab*. Harvard Univ., 26, 141–146.

Liaw J. R. and Matos J. E. (2007) MNSR Flux performance and Core Lifetime Analysis with HEU and LEU fuels. Paper presented at the International Meeting on Reduced Enrichment for Research and Test Reactor held Prague, Czech Republic, September 23 -27

Little R.C., Seamon R.E. (1985) “Nuclear data for MCNP”. In: Alcouffe R., Dautray R., Forster A., Ledanois G., Mercier B. (eds) Monte-Carlo Methods and Applications in Neutronics, Photonics and Statistical Physics. *Lecture Notes in Physics*, vol. 240. Springer, Berlin, Heidelberg

MacFarlane, R.E., Muir, D. W., Boicourt, R. M. Kahler A.C. (2012) “The NJOY Nuclear Data Processing System”, LA-UR-12-27079, Theoretical Division, Los Alamos National Laboratory

Mahmood, T, Pervez S.and Iqbal M., 2008. Neutronic analysis for core conversion (HEU-LEU) of Pakistan Research Reactor-2 (PARR-2). *Annals of Nuclear Energy* 35 pp. 1440 – 1446

Marsaglia, G., (1985), A current view of random number generators, A keynote address, Statistics and Computer Science: XVI Symposium on the Interface, Atlanta, Proceedings, Elsevier.

Matos J. E and Lell R. M, 2005. “Feasibility study of potential LEU fuels for a generic MNSR reactor” A paper presented at the 2005 International meeting on Reduced Enrichment for Research and Test Reactors, November 6 – 10, Boston Massachusetts.

Metropolis, N and Ulam S. 1949 The Monte Carlo Method. *Journal of the American Statistical Association*. Vol 44, No 247. pp. 335-341

Metropolis N, Rosenbluth A. W. Rosenbluth M. N. Teller A. H, Teller, E. 1953 Equation of State Calculations by Fast Computing machines, *The Journal of Chemical Physics*, Vol 21, Number 6, June pp. 1087 - 1092

Muranaka R.G., 1983, "Conversion of research reactors to low-enrichment uranium fuels", *IAEA Bulletin*, Vol.25(1).

Nagaya, Y. Chiba G, Mori T, Irwanto D and Nakajima K. (2010) “Comparison of Monte Carlo calculations methods for effective delayed neutron fraction” *Annals of Nuclear Energy* Vol. 37 pp. 1308 -1315

Nawaz, A., Mirza, S. M., Mirza, N. M., Sohail, M., 2012. Analysis of Core Life-time and Neutronics Parameters for HEU and Potential LEU/MEU Fuels in a Typical MNSR. *Annals of Nuclear Energy*, 47 pp. 46 – 52.

NUREG-1313, (1988). “Safety evaluation report related to the evaluation of low enriched uranium silicide-aluminum dispersion fuel of use in non-power reactors”, US Nuclear Regulatory Commission, July 1988.

Nyarko, B. J. B., Asamoah, M., Akaho, E. H. K.,Yamoah, S., Menshima, E., 2011. Design of Large Irradiation Channel of MNSR Facility in Ghana. *Annals of Nuclear Energy* 38 pp. 431-437.

Omar C, Jean P.P, 1998. Reactor Calculation Using Monte Carlo N-Particle Code, *Algeria Rev. Nuclear Science*, 2 (1): 49-57.

Omar, H., Khattab K, and Ghazi N. (2012) "Feedback reactivity coefficients for the Syrian MNSR research reactor" *Progress in Nuclear Energy* Vol. 54 pp. 162 - 166

Parrish, S., Nicholas, B.,2007. In "Research Reactor Fuel Management and Meeting of the International Group", Centre de Congres, Lyon, France, 11-15th March.

Pond R.B., Hanan N. A, Matos J. E, 2002. Paper presented at the International Meeting on Reduced Enrichment for Research and Test Reactor held at Sancarlos de Bariloche, Argentina 3-8 November. pp. 269-299.

Rozon D., 1998 *Introduction to Nuclear Reactor Kinetics*, Polytechnic International Press, Canada

Ryu., H. O, Kim. Y. S, Park, J. M. Chae, H. T. and Kyu, C. K 2008. Performance Evaluation of U-Mo/Al dispersion fuel by considering fuel-matrix interaction, *Nuclear Engineering and Technology*, Vol 40, No 5, August Issue pp. 409 – 418 Saratoga Springs, New York, May 3-7, 2009

Saidi, P., Sadeghi M and Tenreiro C., 2013. Variance Reduction of Monte Carlo Simulation in Nuclear Engineering Field. *Theory and Applications of Monte Carlo Simulations* – Chapter 7. InTech

Shi, S., 1993. *MNSR Thermal Hydraulics,* MNSR Training Material CIAE, Beijing, China.

Sichani, B. T., Sepanloo, K., Rezvanifard, M., 2006. Neutronic Parameters Survey of LEU – Loaded Iranian MNSR. A paper Presented at the First Research Co-ordination Meeting of the Coordinated Research Project on "Conversion of MNSRs to LEU" Vienna, Austria, 11-14 December.

Shultis, J. Kenneth; Faw, R. E. (2011) *An MCNP Primer*, downloaded from K-State Research Exchange (K-REx), the institutional repository of Kansas State University. K-REx is available at http://krex.ksu.edu

Snoj, L., Kavcic, A., Zerovnik, G., Ravnik, M., 2010.Calculation of Kinetic Parameters for Mixed TRIGA Cores with Monte Carlo. *Annals of Nuclear Energy* Vol. 37 pp. 223-229

Solomon Alvin et al 2002, Thoria-Based Cermet Nuclear Fuel. Proceedings of ICONE10, 10th International Conference on Nuclear Engineering, Arlington VA, April 14 – 18.

Stacey, W. 2001. *Nuclear Reactor Physics*. John Wiley and Sons

Travelli, F. A., 1999. Progress of Reduced Enrichment for Research and Test Reactors Program, Budapest, Hungary, 3-8 October

Trellue, H, Little, R. 2008 "Release of New MCNP S(α,β) Library ENDF70SAB Based on ENDF/B-VII.0", LA-UR-08-3628

Verboomen B, Haeck W and Baeten P, 2006. Monte Carlo calculation of effective neutron generation time, *Annals of Nuclear Energy*, 33 911-916

Verhaegen, Frank and Jan Seuntjens, 2003. Monte Carlo modeling of external radiotherapy photon beams, *Physics in Medicine and Biology*, 48: R107-R164

Waqar S, Mirza S. M, Mirza N. M and Asad. T. 2008. "A comparative study of the standard HEU core and various potential LEU alternatives for a typical MNSR system" *Nuclear Engineering and Design*, Vol 238. pp2302-2307

X-5 Monte Carlo Team, 2003. *MCNP—A General Monte Carlo N-Particle Transport Code*, Version 5, LA-CP-03-0245, Los Alamos National Laboratory, USA

Yang Y. W., 1992. *MNSR Reactor Complex Manual*, China Institute of Atomic Energy, Beijing, China.